Modeling the water isotopes in Greenland precipitation 1959–2001 with the meso-scale model REMO-iso

J. Sjolte, G. Hoffmann, S. Johnsen, B. Vinther, Valérie Masson-Delmotte, C. Sturm

Modeling the water isotopes in Greenland precipitation 1959–2001 with the meso-scale model REMO-iso

J. Sjolte,[1] G. Hoffmann,[2,3] S. J. Johnsen,[1] B. M. Vinther,[1] V. Masson-Delmotte,[2] and C. Sturm[4]

Received 4 November 2010; revised 19 June 2011; accepted 7 July 2011; published 21 September 2011.

[1] Ice core studies have proved the $\delta^{18}O$ in Greenland precipitation to be correlated to the phase of the North Atlantic Oscillation (NAO). This subject has also been investigated in modeling studies. However, these studies have either had severe biases in the $\delta^{18}O$ levels, or have not been designed to be compared directly with observations. In this study we nudge a meso-scale climate model fitted with stable water isotope diagnostics (REMO-iso) to follow the actual weather patterns for the period 1959–2001. We evaluate this simulation using meteorological observations from stations along the Greenland coast, and $\delta^{18}O$ from several Greenland ice core stacks and Global Network In Precipitation (GNIP) data from Greenland, Iceland and Svalbard. The REMO-iso output explains up to 40% of the interannual $\delta^{18}O$ variability observed in ice cores, which is comparable to the model performance for precipitation. In terms of reproducing the observed variability the global model, ECHAM4-iso performs on the same level as REMO-iso. However, REMO-iso has smaller biases in $\delta^{18}O$ and improved representation of the observed spatial $\delta^{18}O$-temperature slope compared to ECHAM4-iso. Analysis of the main modes of winter variability of $\delta^{18}O$ shows a coherent signal in Central and Western Greenland similar to results from ice cores. The NAO explains 20% of the leading $\delta^{18}O$ pattern. Based on the model output we suggest that methods to reconstruct the NAO from Greenland ice cores employ both $\delta^{18}O$ and accumulation records.

Citation: Sjolte, J., G. Hoffmann, S. J. Johnsen, B. M. Vinther, V. Masson-Delmotte, and C. Sturm (2011), Modeling the water isotopes in Greenland precipitation 1959–2001 with the meso-scale model REMO-iso, *J. Geophys. Res.*, *116*, D18105, doi:10.1029/2010JD015287.

1. Introduction

[2] The Greenland ice sheet is of particular interest for climate studies, both concerning recent changes and on longer time scales. The growing number of ice cores from the Greenland ice sheet now produces a versatile picture of the Greenland climate history with sufficient spatial resolution to capture regional differences [*Vinther et al.*, 2010; *Masson-Delmotte et al.*, 2005; *Bales et al.*, 2009]. One of the primary parameters for determining the rate and magnitude (in terms of temperature and circulation) of past climate and water cycle changes is the analysis of $\delta^{18}O$ and δD.

[3] *Dansgaard* [1953] showed that the relative abundance of ^{18}O in precipitation, commonly expressed as $\delta^{18}O$, is related to the condensation temperature due to the less volatile $H_2^{18}O$ molecules condensating more readily than the $H_2^{16}O$ molecules. Following an air parcel being cooled, e.g. being displaced to the north, the vapor pressure decreases with temperature and as a result the $\delta^{18}O$ of the condensate decreases as the distillation progresses. This concept has been used in one dimensional distillation models to explore the relationships between the $\delta^{18}O$ and temperature in polar areas [*Johnsen et al.*, 1989; *Ciais and Jouzel*, 1994], and in a more elaborate back-trajectory study by *Sodemann et al.* [2008].

[4] In this introduction section, we briefly review the modeling of stable isotopes in global atmospheric models (Section 1.1) and regional models (Section 1.2) before describing the structure of the manuscript.

1.1. Stable Isotope Modeling Using Climate Models

[5] The first implementation of isotope diagnostics in a General Circulation Model (GCM) was done by *Joussaume et al.* [1984]. Since then a number of global models have been fitted with isotope modules enabling the computation of the isotopic composition through each part of the hydrological cycle [e.g., *Jouzel et al.*, 1987; *Hoffmann et al.*, 1998; *Mathieu et al.*, 2002; *Noone and Simmonds*, 2002; *Yoshimura et al.*, 2008; *Risi et al.*, 2010]. Isotope enabled GCMs have been used in studies of the past climate to interpret the findings

[1]Centre for Ice and Climate, Niels Bohr Institute, Copenhagen, Denmark.
[2]LSCE (CEA-CNRS-UVSQ-IPSL), CEA Saclay, Gif sur Yvette, France.
[3]Now at Institute for Marine and Atmospheric Research Utrecht, Utrecht University, Utrecht, Netherlands.
[4]Bert Bolin Centre for Climate Research, Institute for Geology and Geochemistry, Stockholm University, Stockholm, Sweden.

0148-0227/11/2010JD015287

in isotopic archives in terms of temperature, precipitation and atmospheric circulation. These studies include the seasonality and origin of polar precipitation for the last glacial maximum (LGM) [*Werner et al.*, 2000, 2001], the temperature-isotope relationship of past climates [*Jouzel et al.*, 2000] and the δ^{18}O of precipitation in monsoon areas for LGM and the Eemian interglacial [*Hoffmann and Heimann*, 1997; *Herold and Lohmann*, 2009].

[6] Recent studies [*Yoshimura et al.*, 2008; *Risi et al.*, 2010] have focused on forcing isotopic GCMs with meteorological reanalysis data to obtain realistic weather patterns, and thereby being able to evaluate the reproducibility of the observed isotopic signal more strictly. While both of these studies compared the model output with time series of observed weather data and measured δ^{18}O for the tropics and mid-latitudes, none of them performed an in-depth analysis of variability and coherency between models and data over Greenland.

[7] Studies of Greenland ice cores shown the δ^{18}O and/or accumulation of selected sites to be correlated to the North Atlantic Oscillation (NAO) [e.g., *White et al.*, 1997; *Appenzeller et al.*, 1998; *Vinther et al.*, 2003]. Subsequently has the influence of the NAO on the Greenland δ^{18}O and precipitation amount also been investigated in model studies. In a simulation with the isotope enabled version of the European Centre Hamburg Model version 4 (ECHAM4-iso), forced with observed sea surface temperatures (SSTs) for 1950–1994, *Werner and Heimann* [2002] found the δ^{18}O in precipitation and the precipitation amount in western Greenland to be negatively correlated to the modeled NAO index. Forcing a GCM with observed SSTs does not generate a simulation where the actual weather patterns are reproduced. Hence, *Werner and Heimann* [2002] only concluded that the modeled range of δ^{18}O variability over Greenland was realistic, and did not attempt to correlate the model output directly to observations. Although not using a GCM model, *Sodemann et al.* [2008] coupled an isotope distillation model with back-trajectories forced by reanalysis data, and also found the δ^{18}O in precipitation to be out of phase with the NAO. Specifically, the winter δ^{18}O was estimated to be 3.8 ± 6.8‰ lower during positive phase NAO than during negative phase NAO [*Sodemann et al.*, 2008]. However, when compared directly to the δ^{18}O of ice core records the method of *Sodemann et al.* [2008] overestimated the winter values by ~13–14‰.

1.2. Regional Modeling of Stable Isotopes

[8] The typical low resolution of global models has motivated isotope diagnostics to be fitted in higher resolution regional climate models, with the benefits of better representation of cyclonogenesis, vapor advection and orography to follow. For the Greenland ice sheet, the spatial distribution of precipitation is a result of moist air over the open North Atlantic Ocean being forced over the steep topography by cyclonic flow [*Schuenemann et al.*, 2009]. *Kiilsholm et al.* [2003] showed that more realistic precipitation patterns for Greenland could be achieved using a regional model than with a coarser resolution global model. The model performance for the δ^{18}O of precipitation, being closely linked to the rain-out process, is expected to improve with resolution as well. Besides the improved performance for precipitation by using a regional model, spatial features are represented in greater detail than with a global model. This is especially desirable for areas not covered by ice core or observational data. As noted in the study of a short-term synoptic scale event by *Yoshimura et al.* [2010] using the isotopic regional spectral model (IsoRSM), there are only two existing isotopic regional climate models, one being REMO-iso and the other being IsoRSM. The REMO (REgional MOdel) climate model was developed from the Europa-Modell forecast model of the Deutscher Wetterdienst [*Majewski*, 1991]. Initially it was the result of the Europa-Modell being modified to work both in forecast mode and in climate model mode by *Jacob and Podzun* [1997]. Later on REMO was updated with ECHAM4 physics parameterizations, and used to study the water budget in the Baltic region [*Jacob*, 2001]. Most relevant to this study, REMO was also optimized (updated to version 5.0) and validated for use in Arctic regions by *Semmler* [2002]. These optimizations include fractional sea ice, realistic snow melt and ground moisture and improved cloud representation. REMO does not compute explicit snow surface processes such as snow drift, wind erosion and percolation of melt water in the snow pack. The first experiments with REMO-iso were carried out over Europe and South America [*Sturm et al.*, 2005, 2007]. In these areas REMO-iso was able to successfully simulate annual and monthly mean isotopic compositions of precipitation compared to observations. Moreover, REMO-iso performed significantly better in comparison with results from lower resolution models, especially in reproducing precipitation patterns [*Sturm et al.*, 2007].

[9] In this paper we present the results of the first study focused on Greenland using a regional climate model fitted with isotope diagnostics. The aim is to investigate the influence of the NAO on the temporal and spatial variability of the δ^{18}O in Greenland precipitation. Our approach is to nudge REMO-iso to follow the observed weather patterns (see Section 2.1 for details). In theory, if the weather patterns are reproduced by REMO-iso, the modeled isotope output should be close to the δ^{18}O from ice cores and instrumental data series. The model experiment is based on the ERA-40 reanalysis covering the period 1958–2001. We will first evaluate the performance of REMO-iso over Greenland and the North Atlantic area using isotopic Global Network In Precipitation (GNIP) and ice core data. This includes an evaluation of the performance of REMO-iso in terms of annual mean temperature, precipitation and δ^{18}O, and analyses of the temporal and spatial relation between temperature and δ^{18}O. Furthermore, we will evaluate the modeled interannual variability of temperature, precipitation and δ^{18}O in comparison with meteorological observations and ice core data, emphasizing the distinction between the performances for summer and winter. As a part of the model evaluation we will compare the performance of the REMO-iso regional model to the performance of the ECHAM4-iso global model (see also auxiliary material), and assess the benefits of using a regional model versus a global model.[1] Finally, we will investigate what drives the large scale interannual variability in summer and winter δ^{18}O through i) an analysis of the main

[1] Auxiliary materials are available in the HTML. doi:10.1029/2010JD015287.

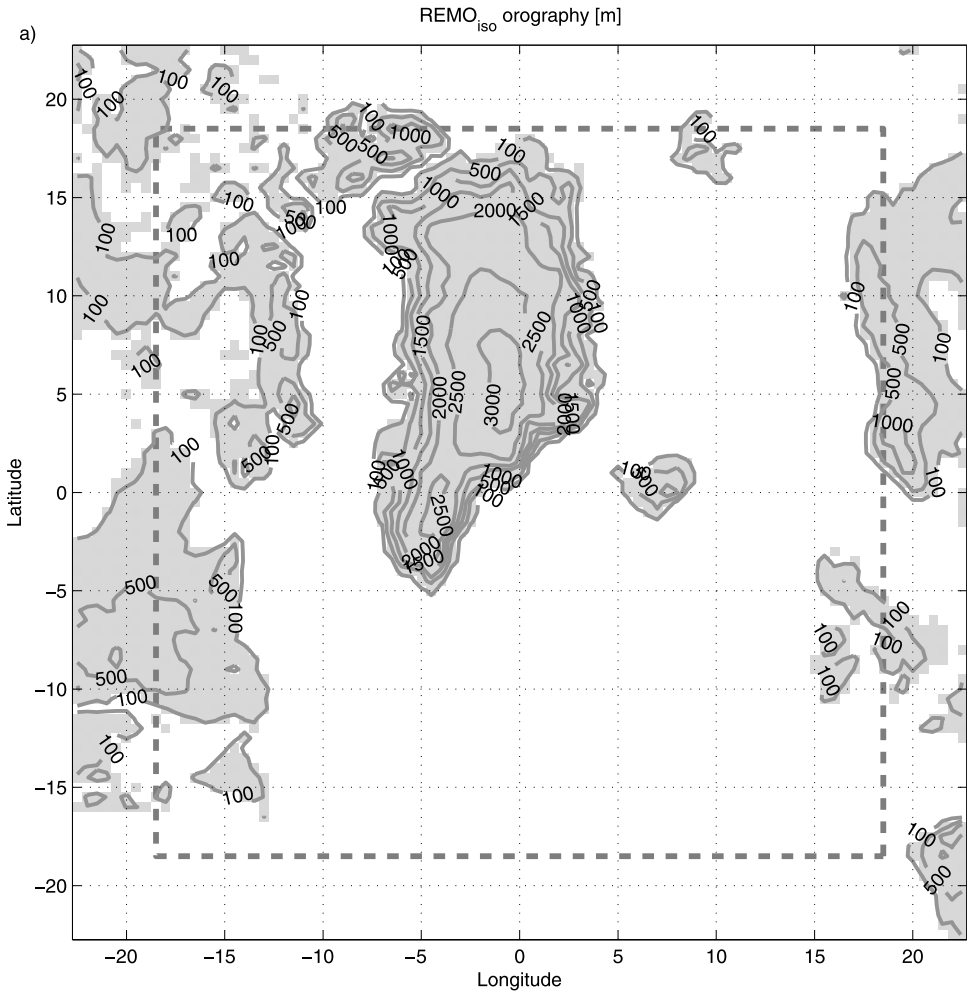

Figure 1. Model domain land-sea mask (shaded) and orography [m] for REMO-iso in rotated coordinates. The model grid is 91 × 91 grid boxes with 0.5° or ~55 km resolution. The dashed line marks the extent of the model domain without the 8 grid box wide buffer zone.

patterns of variability for the modeled temperature, $\delta^{18}O$ and precipitation, ii) the connection between these patterns and the NAO, and iii) the temporal persistency of the influence of the NAO.

2. Data and Methods

2.1. Experiment Setup

[10] We use REMO-iso in a domain of 91 × 91 grid points with the standard resolution of 0.5° (longitude/latitude), 19 vertical layers with the lowest level at ~50 m, and a time step of 5 minutes. The model domain is zoomed on Greenland and the surrounding North Atlantic (see Figure 1). The simulation is initialized on a rotated grid, with the Equator passing through the center of the domain. This means that the high and low latitudes are numerically represented in approximately the same spatial resolution. The model run spans 44 years using the meteorological conditions and SSTs from the reanalysis product ERA-40 of the European Center of Medium-Range Weather Forecasts (ECMWF) covering the time period 1958–2001 [*Uppala et al.*, 2005]. The ERA-40 reanalysis has been found to be reliable for the high latitudes in the Northern Hemisphere for the entire reanalysis period [*Bromwich et al.*, 2007], and to correspond well to independent observations in the Arctic [*Bromwich and Wang*, 2005]. Compared to the NCEP-NCAR reanalysis, the ERA-40 reanalysis has greater strong-cyclone activity in the extratropics, which is attributed to the higher spatial resolution and better assimilation scheme of the ERA-40 reanalysis [*Wang et al.*, 2006]. The first year of the model run is considered a spin up year, and is not used for the analysis. To provide the lateral boundary conditions for the regional model we first run the global model ECHAM4 fitted with water isotope diagnostics [*Hoffmann et al.*, 1998] in a spectral resolution of T42 (2.5° × 2.5°) also using the ERA-40 reanalysis. To approach the actual weather patterns of the simulated period both the regional and the global model are run using a nudging technique [*Jeuken et al.*, 1996]. For the global model this means that for every six hours the temperature and the wind field are relaxed towards the temperature and the wind field of the ERA-40 reanalysis, while for the regional model the wind field is relaxed towards the wind field of the global model. In short, the nudging involves adding a small term to the tendency in the field calculated by the model, such that

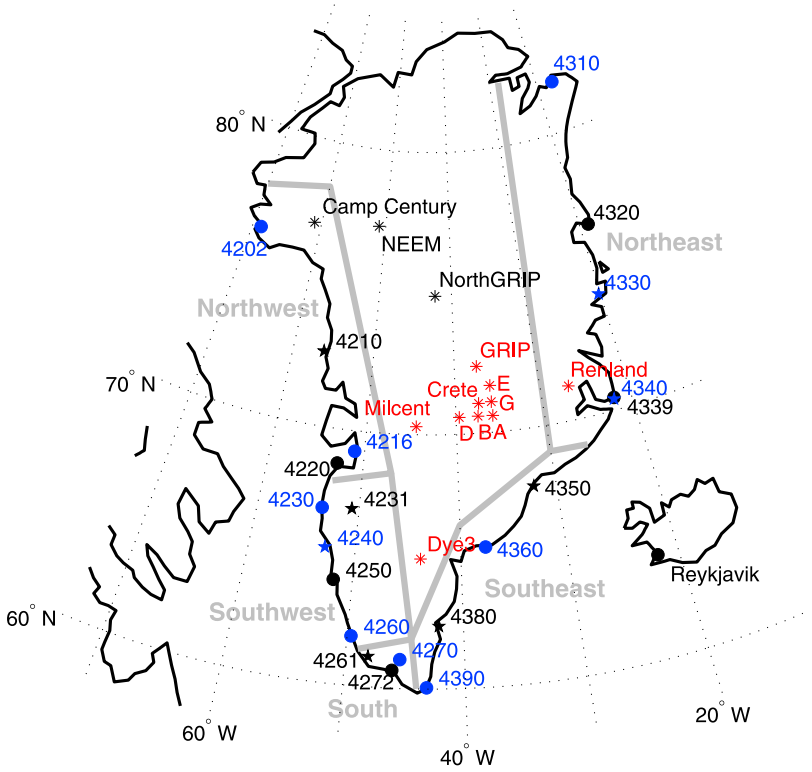

Figure 2. Numbered DMI coastal stations marked with blue/black dots for stations with both temperature and precipitation data, while stations with only climatological monthly precipitation data are marked with blue/black stars. The blue/black color distinction is made to more easily tell the different stations apart. Data are available from http://www.dmi.dk. Ice core sites are marked with asterisks, with the sites used in this study marked in red. Also marked are the areas defining the coastal regions used in Figure 4.

the model is forced towards field of the reanalysis. We use a spectral nudging technique for the regional model, where only the upper level flow is affected by the nudging [*von Storch et al.*, 2000]. With these differences in nudging techniques, the regional model is more loosely constrained relative to the reanalysis. While this takes advantage of the high resolution of the regional model, it can also lead to less coherency between observed variability and the modeled variability of REMO-iso. As an alternative to nudging, an ensemble experiment, similar to the procedure for regional weather forecasting, would allow for a direct comparison to observations and ice core data [*Leutbecher and Palmer*, 2008]. However, this would require multiple model runs with an already computational demanding regional model.

[11] In summary, the circulation information of the ERA-40 reanalysis is passed on to the regional model in two ways: First, the lateral boundary conditions of REMO-iso are prescribed using the corresponding prognostic variables (that is wind, temperature, humidity, water isotopes) from ECHAM4-iso, which is already nudged to the reanalysis wind field. Over a buffer zone of 8 horizontal layers from the outer boundary this synoptic information is introduced into REMO-iso (see Figure 1). Secondly, within the domain REMO-iso is nudged to the wind field of the global simulation. All other prognostic parameters (temperature, humidity etc.) of REMO-iso including the water isotopes are calculated independently.

2.2. Observational and Ice Core Data

[12] The monthly meteorological Greenland data used in the model-data comparison of this study are provided by the Danish Meteorological Institute (DMI) [*Cappelen et al.*, 2001; *Joergensen and Laursen*, 2003], and locations of the coastal meteorological stations and major inland ice core drilling sites are indicated in Figure 2. The coastal temperature and precipitation records cover the period 1959 to 1999, with only few missing months of data. For the stations numbered 4210, 4231, 4240, 4261, 4330, 4340, 4350 and 4380 only climatological monthly means are available from DMI. Data from these stations (marked with stars in Figure 2) will only be used in the evaluation of the modeled mean annual cycle of precipitation.

[13] Seasonal mean $\delta^{18}O$ values for 10 ice core sites have been calculated by *Vinther et al.* [2010]. This includes four cores from the Dye-3 site and six cores from Summit. Except for the Dye-3 and Renland sites, the ice core data have been corrected for post depositional diffusion. Isotopic diffusion in the firn progressively reduces the seasonal amplitude. In a first step *Vinther et al.* [2010] therefore reconstructed the original amplitude at most sites by a numerical back-diffusion approach [*Johnsen*, 1977]. Due to the presence of melt layers at two sites (Dye-3 and Renland) this approach would lead to major inconsistencies and a modified technique was applied for these sites (for details see *Vinther et al.* [2010]). In the next step, winter and summer signals were defined dividing the year in two seasons only. The dating of the ice cores was

Table 1. List of GNIP Stations Used in This Study and the Time Period Covered by Monthly Sampling[a]

Station Name	Site Identification	Longitude	Latitude	Time Period
Ny Ålesund	100400	11.56°E	78.15°N	1990–2007
Reykjavik	403000	21.93°W	64.13°N	1961–1969 1973–1976 1992–2006
Thule	420200	68.83°W	76.52°N	1966–1972
Gronnedal	426100	48.12°W	61.22°N	1961–1970
Station Nord	431000	16.67°W	81.60°N	1961–1968 1971–1972
Danmarkshavn	432000	18.66°W	76.76°N	1991–2007
Scoresbysund	434001	22.00°W	70.50°N	1961–1965
Prins Chr. Sund	439000	43.11°W	60.03°N	1976–1978

[a]See IAEA Isotope Hydrology Information System (ISOHIS) online data (2006).

done by defining the $\delta^{18}O$ maximum and minimum to be in July/August and January/February, respectively. *Vinther et al.* [2010] then assumed a uniform year round precipitation distribution, attributing half of the annual precipitation to each season. This means that summer corresponds to the period May to October and winter to the period November to April. Though this approach depends on the approximate stability of seasonal precipitation, *Vinther et al.* [2010] showed that the seasonal isotope records are precise enough to allow for a quantitative comparison with meteorological observations.

[14] In addition to the ice core data, GNIP $\delta^{18}O$ data are used for the model validation. This includes climatological means from station on the Greenland coast, Iceland and Svalbard (see Table 1 for details). In this study the modeled data are interpolated to the site coordinates whenever comparing to specific station or ice core data.

[15] To assess the quality of the accumulation on the Greenland ice sheet as calculated by REMO-iso, the Program for Arctic Regional Climate Assessment (PARCA) accumulation data set is introduced. The PARCA data set [*Bales et al.*, 2001] is a gridded spatial distribution of accumulation based on interpolation of over 200 shallow ice cores, snow pits and meteorological station data producing a high resolution map for the period 1971 to 1990.

[16] The NAO index is traditionally defined as the pressure difference between Iceland and the Azores [*Walker and Bliss*, 1932]. In this paper, we use the NAO index defined as the normalized pressure difference between Gibraltar and a composite of data from stations in the southwest of Iceland [*Jones et al.*, 1997]. Monthly data until the year 2000 can be downloaded from the web page of the Climate Research Unit (http://www.cru.uea.ac.uk/cru/data/nao/).

3. Results

3.1. Climatology

[17] In this section we evaluate the model skill for temperature, precipitation and $\delta^{18}O$ in precipitation with respect to the long term observed climatology. Similarly to other climate models, REMO-iso and ECHAM4-iso have a warm bias over the ice sheet [*Walsh et al.*, 2008]. For example, the modeled annual mean temperature for the Summit station is −25°C and −27°C for REMO-iso and ECHAM4-iso, respectively, while the observed mean temperature is reported to be −32°C [*Johnsen et al.*, 1992]. The ERA-40 reanalysis, to which ECHAM4-iso temperature is nudged, also has a warm bias for Summit with an annual mean temperature of −28°C. These warm biases are similar to the results of a SST forced GCM experiment for 1950 to 1994 by *Werner and Heimann* [2002] using the same global model (ECHAM4) as in this study. For this study the height anomalies between the models and the actual site (−96 m and −121 m, for REMO-iso and ECHAM4-iso respectively), are relatively small, and other factors such as misrepresentation of the surface temperature inversion or albedo must be responsible for these significant biases in the modeled temperature. For REMO-iso the overestimated temperatures are most pronounced at high and intermediate altitude on the ice sheet. Moreover, this model deficiency is much stronger in the Northern and Central Part of the ice sheet and hardly significant in the South. The bias becomes particularly strong during summer time and is approximately +3°C in Southern Greenland and up to +7°C in the North. For the coastal areas the simulated temperature is generally too cold by a few degrees compared to DMI station data, with the largest cold bias during winter. For some stations this cold bias can be explained partly by model orography, but the tendency also exists where there are only negligible differences between the model and the observed elevation. Other effects specifically important to the climate on the edge of ice sheets, such as misrepresentation of katabatic winds, might be responsible for this.

[18] The fact that the model bias peaks during summer times points to possible problems with the computed surface albedo. REMO-iso computes a varying snow albedo (fresh snow having a higher albedo) allowing for a maximum albedo of 0.8, whereas most observations indicate higher values of about 0.85 [*Box et al.*, 2006]. In a study of the Arctic boundary layer by *Tjernstrom et al.* [2005], REMO was reported to have temperature biases linked to the surface radiation budget mentioning cloud representation and surface albedo as the causes. The biases found were a −2°C surface temperature bias during summer and autumn, and a bias of up to +2°C in the lower troposphere above 2 km for spring, summer and autumn. The biases found by *Tjernstrom et al.* [2005] do not correspond directly to the biases found for Greenland in this study. However, it should be kept in mind that the *Tjernstrom et al.* [2005] study was carried out over the Arctic Ocean, and the biases do not necessarily translate between regions. *Box and Rinke* [2003] also found a warm bias in their simulation with the High-Resolution Limited Area Model (HIRHAM), and rather than the albedo being the problem, pointed out the importance of a realistic description of the boundary layer over the ice sheet.

3.1.1. Spatial Variations in Greenland Accumulation

[19] The spatial pattern and absolute amount of precipitation is important for the surface mass balance of the ice sheet. The modeled accumulation depends on the interplay of

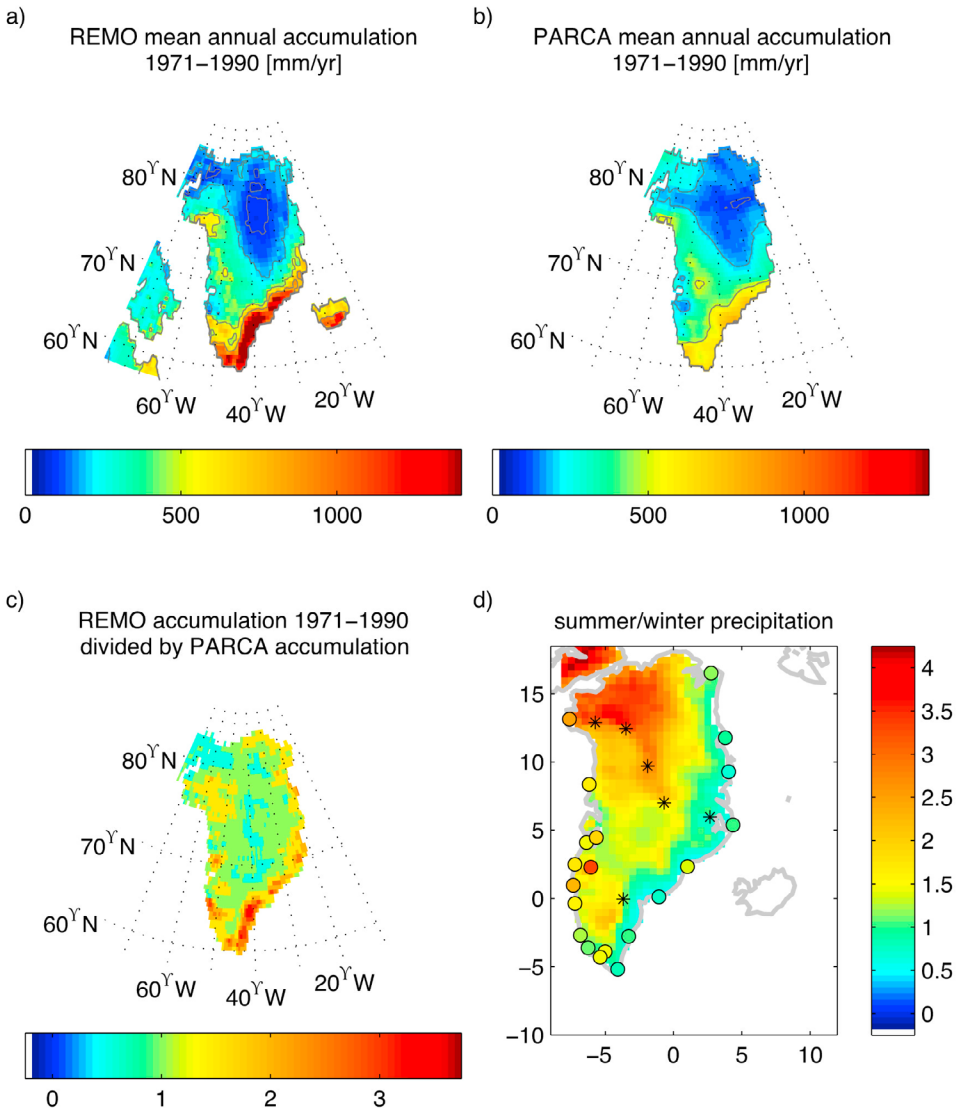

Figure 3. (a) REMO-iso accumulation (P-E) [mm/yr] compared with (b) the PARCA accumulation map [mm/yr]. Both data sets have been interpolated to a 0.5° × 0.5° geographical grid. The raw PARCA data are in a 5 km UTM grid. In Figures 3a and 3b the same color bar is used and contour lines are drawn for 100, 200, 500 and 800 mm/yr to ease comparison. In fact, the maximum values for Figure 3a is more than 2000 mm/yr, while the maximum in Figure 3b only is about 800 mm/yr. (c) The differences in magnitude: REMO-iso accumulation divided by PARCA accumulation both annually averaged for the period 1971–1990. Each color on the map in Figure 3c signifies that the model will be within ±25% of a given multiple of the PARCA data. (d) Modeled summer precipitation (May-Oct) divided by winter precipitation (Nov-April) with observations from coastal stations indicated by the colored dots. A map of the ECHAM4-iso accumulation can be found in the auxiliary material (Figure S1).

many factors such as realistic storm tracks, a well resolved orography, a realistic lapse rate over the ice sheet or a realistic large scale moisture transport, which is in our case controlled by the global model ECHAM4-iso. Figure 3 shows the simulated accumulation (Precipitation-Evaporation) compared to the climatological PARCA accumulation map [*Bales et al.*, 2001].

[20] REMO-iso reproduces many features of the spatial accumulation such as the large maximum along the southeastern coast of Greenland and the minor local maximum southwest of Pituffik/Thule (station 4202 in Figure 2). These maxima are controlled by the principal entrance points of North-Atlantic storm tracks on the Greenland ice sheet. Also the large very dry area in the central and northeastern parts of the ice sheet is captured by the model. The PARCA accumulation map shows a latitudinal gradient calculated over equal areas from 558 mm/yr about 65°N (Dye-3) to 194 mm/yr east of Camp Century (77°N), corresponding to a reduction of accumulation over the ice sheet by a factor of 2.9. REMO-iso has a stronger latitudinal gradient in accumulation, with 1026 mm/yr for the southern area to 226 mm/yr in the northern area. This is a reduction by a factor of 4.5.

[21] The model produces too little precipitation in central regions of the ice sheet, where the accumulation is underestimated by about 25%. For reference the ERA-40 reanalysis underestimates the inland precipitation by up to 50% [*Bromwich et al.*, 2007]. In some areas towards the coast REMO-iso overestimates the amount of accumulation by about 50%. This is also seen in the comparison with the observed DMI coastal data discussed in Section 3.1.2. However, the large overestimation for the southeastern maximum compared to the PARCA accumulation is probably an artifact. The PARCA accumulation study is focusing on the interior of the ice sheet and the data set was constructed to better understand ice sheet dynamics. Coastal areas however, are not represented in detail [*Bales et al.*, 2001]. When comparing the PARCA data with the DMI weather stations, much higher accumulation is found for a number of these coastal sites (PARCA maximum in the Southeast: 800 mm/yr, DMI station 4390 (see Figure 2): 1900 mm/yr).

[22] In the Third Assessment Report of the Intergovernmental Panel on Climate Change (IPCC) the best estimate of the total accumulation (P-E) over Greenland was 225 ± 41 mm/yr considering the spread between about a dozen studies [*Church et al.*, 2001]. The PARCA data set gives a total accumulation value of 300 ± 80 mm/yr. Former modeling studies underlined the importance of numerical resolution to achieve realistic values of the total accumulation. *Kiilsholm et al.* [2003] showed an improvement in the simulated total accumulation from 421 ± 183 mm/yr (in the following ± refers to the standard deviation of interannual variability) using the Max Planck Institute for Meteorology coupled ocean atmosphere general circulation model ECHAM4/OPYC model (~300 km resolution) to a more realistic 224 ± 35 mm/yr using a regional climate model, HIRHAM at ~50 km resolution in an approach similar to this study with the REMO-iso regional model. Here both models, the global and the regional model, were nudged to guarantee a realistic circulation pattern over the simulated interval. For the period 1960–1990 REMO-iso and ECHAM4-iso produce a mean accumulation of 353 ± 78 mm/yr and 336 ± 67 mm/yr, respectively. Although this is less than the value for ECHAM4/OPYC mentioned above, it is still an overestimation of the accumulation compared to PARCA accumulation data set and the study by *Church et al.* [2001].

[23] The dry bias for cold regions found for the central northern Greenland is not something unique to REMO-iso as a climate model. *Masson-Delmotte et al.* [2008] found a dry bias for inland Antarctica in a study of three GCMs (ECHAM4, MUGCM, GISS-E). This was attributed to an underestimation of the vapor transport to the cold regions. *Kiilsholm et al.* [2003] showed similar accumulation rates as REMO-iso for inland Greenland, using the HIRHAM regional model in a 50 km resolution, while *Box et al.* [2006] did not report a dry bias for the Polar MM5 regional model in a 24 km resolution. This could suggest that even higher resolution than the ~55 km used in this REMO-iso simulation is needed to reach proper accumulation rates in cold regions, although difference in model physics also could explain these differences.

3.1.2. The Seasonal Cycle for Precipitation

[24] In the following, the simulated precipitation amount and seasonal cycle is evaluated using observed DMI precipitation data for the period 1961 to 1990. It should be noted that most of the stations have single or multiple missing monthly values in the period 1961 to 1990 (see also Section 2.2).

[25] The water isotopes undergo a pronounced seasonal cycle (in the order of 15‰ in the interior of the ice sheet for $\delta^{18}O$) and each bias in the seasonality of accumulation has a direct consequence on the mean isotope signal. It is therefore important to evaluate the capability of the model to simulate the regionally varying seasonal precipitation cycle. The various meteorological stations were divided in five groups considering geographical positions and similarities in the annual cycle of precipitation (see Figure 2). In Figure 4 the modeled and observed seasonal cycle for five Greenland regions is plotted. The agreement between the model and the observations is good. See in particular the late summer/autumn maximum in the Northwest and the pronounced summer minimum in the Southeast both captured by REMO-iso. The evaluation of the annual cycle for precipitation for coastal regions shows that REMO-iso captures the observed regional contrast.

[26] However, it is the annual cycle for inland Greenland and the question of the precipitation weighting of the mean annual $\delta^{18}O$ that is relevant for ice core and modeling studies of the past climate [*Masson-Delmotte et al.*, 2005; *Werner et al.*, 2000]. In Figure 3d a map of the summer divided by winter precipitation is plotted together with the observed data. For this comparison the evaporation is disregarded, assuming that the precipitation has the largest contribution in determining the annual cycle of accumulation, and to be able to compare to the meteorological observations. The map in Figure 3d shows large regional differences in the seasonal distribution of precipitation. To a large extent the modeled seasonal contrast of precipitation in the inland regions follows the coastal pattern, with an overweight of winter precipitation in the southwest and an overweight of summer precipitation towards the northeast. Additional to this overall pattern an area with relative little winter precipitation extends from the northwestern Greenland all the way to central sites such as the Summit region. While there are not sufficient observational data to confirm the modeled pattern of seasonality for the interior of the ice sheet, studies of ice cores at Summit [*Shuman et al.*, 1995] and in the North Greenland Ice core Project (NGRIP) region [*Shuman et al.*, 2001] both show an overweight of summer precipitation. Also, in *Steen-Larsen et al.* [2011] the ratio between summer and winter precipitation is shown for REMO-iso along with five other climate models, four of which are showing a similar seasonal contrast in precipitation. If this modeled pattern of the spatial distribution of the seasonal contrast in precipitation is realistic, then there are large differences in the seasonal biases dominating the annual signal recorded in the $\delta^{18}O$ for different regions in Greenland.

3.1.3. Isotope Climatology

[27] Comparing the seasonal mean isotope levels for the 10 ice core sites (see Table 2) REMO-iso produces a positive bias in $\delta^{18}O$ of about 2–3‰ during winter and 5–6‰ during summer resulting in an annually weighted overestimation of 4.4‰. In the case of Renland the positive bias is even greater very likely due to the model orography, where the Renland site is almost 1300 m too low compared with the actual site elevation. For all sites REMO-iso is closer to the annual mean ice core $\delta^{18}O$ than ECHAM4-iso by at least 1–2‰. By using the modeled $\delta^{18}O$ lapse rate we can estimate

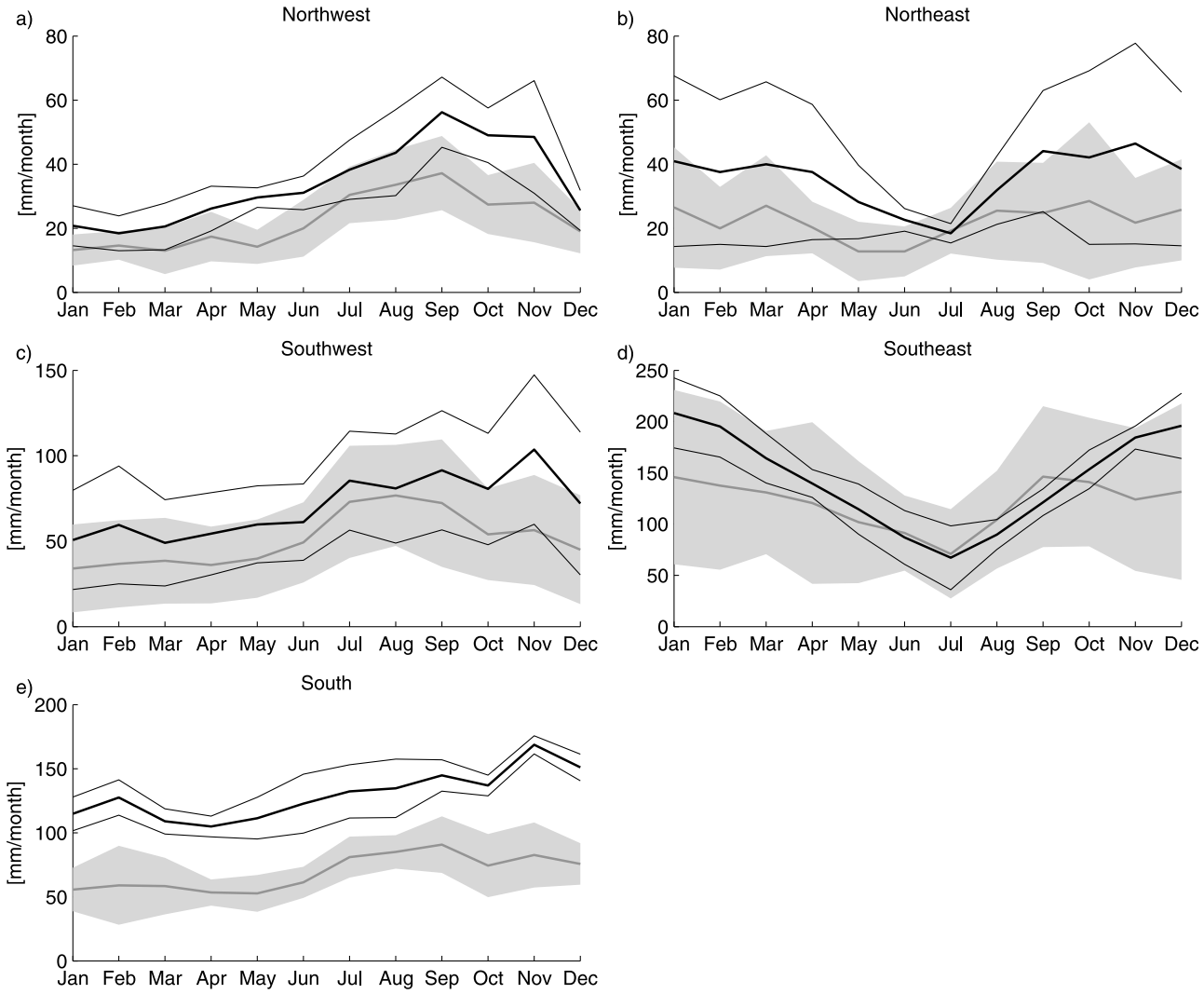

Figure 4. Observed and modeled annual cycle for precipitation averaged for 5 coastal regions as defined in Figure 2. The time period is 1961–1990. Stations 4210, 4216, 4231, 4240, 4261, 4330, 4340, 4350 and 4380 (see Figure 2): only provisional data exists. Model data are in black with the thin lines indicating one standard deviation and the observed data are in gray with the shaded area indicates one standard deviation for the spread between the station data.

Table 2. Seasonal and Annual δ^{18}O Values for Ice Core ($\delta^{18}O_{ic}$), the Differences Between REMO-iso and Ice Core δ^{18}O ($\Delta\delta^{18}O_{re\text{-}ic}$), and the Differences Between ECHAM4-iso and Ice Core δ^{18}O ($\Delta\delta^{18}O_{ec\text{-}ic}$)[a]

Site	$\delta^{18}O_{ic}$ Sum/Win	$\Delta\delta^{18}O_{re\text{–}ic}$ Sum/Win	$\Delta\delta^{18}O_{ec\text{-}ic}$ Sum/Win	$\Delta\delta^{18}O_{re\ -\ ic}$ Annual	$\Delta\delta^{18}O_{ec\text{–}ic}$ Annual	Elevation (m a.s.l.)	$\Delta elev_{re}$	$\Delta elev_{ec}$
Crete	−32.4/−36.0	6.6/2.7	6.6/2.9	4.8	6.1	3172	−96	−139
Dye-3 stack	−27.0/−28.7	5.8/3.2	8.8/7.9	4.6	8.5	2480	−65	−845
Summit stack	−31.8/−37.8	5.4/3.0	4.5/2.5	4.7	5.0	3238	−96	−121
Milcent	−26.9/−31.2	4.8/2.7	4.4/2.5	3.8	4.7	2410	69	−156
Renland	−26.4/−28.1	8.4/2.7	9.1/6.8	7.0	8.4	2350	−1298	−1205
Site A	−30.9/−35.3	4.8/1.3	6.9/1.3	3.4	6.9	3092	−36	−358
Site B	−31.0/−35.8	5.3/2.4	6.0/2.8	4.0	6.2	3138	−73	−227
Site D	−29.7/−34.6	5.2/2.9	4.2/2.9	4.0	4.4	3018	−26	5
Site E	−32.0/−37.8	5.8/3.5	6.3/3.4	4.9	6.7	3087	−30	−152
Site G	−31.5/−36.8	5.4/2.6	6.4/2.8	4.7	6.7	3098	−24	−207

[a]The differences are calculated as model output minus ice core values. In the second through fourth columns the first number is for summer means (sum) and the second number is for winter means (win). Also listed is the elevation for each site and the deviation between this and the model orography of REMO-iso ($\Delta elev_{re}$) and ECHAM4-iso ($\Delta elev_{ec}$).

Table 3. The δ^{18}O Lapse Rate (‰/100 m) Calculated for Greenland GNIP and Ice Core Sites (GNIP/Ice Core Sites) and All of Greenland (Greenland Grip Points (Models))[a]

Data Source	GNIP/Ice Core Sites	Greenland Grid Points (Models)
GNIP/ice core obs.	−0.63 ± 0.03	
REMO-iso	−0.58 ± 0.02	−0.41 ± 0.01
ECHAM-iso	−0.53 ± 0.02	−0.39 ± 0.01

[a]The δ^{18}O has been corrected for the latitudinal dependence prior to calculating the lapse rates.

how much of the bias is caused by the orography in the models. The modeled and observed δ^{18}O lapse rates are listed in Table 3. For the Greenland GNIP and ice core sites only, the δ^{18}O lapse rates for both REMO-iso and ECHAM4-iso are slightly underestimated compared to the observed lapse rate. Furthermore, the modeled lapse rates calculated using grid points for all of Greenland are lower than the lapse rates calculated using the Greenland GNIP and ice core sites only. This suggests that the lapse rate of ~−0.6‰/100 m could be overestimated due to the limited coverage of the observations. For REMO-iso less than 0.5‰ of the biases in the annual mean δ^{18}O can be explained by model orography using the modeled lapse rate of −0.41‰/100 m, except for the Renland site where 5.3‰ can be explained by model orography. For ECHAM4-iso less than 1.0‰ of the biases in the annual mean δ^{18}O can be explained by model orography using the modeled lapse rate of −0.39‰/100 m, except for Dye-3, Renland and Site A, where 3.3‰, 4.7‰ and 1.4‰ can be explained by model orography, respectively. It should be kept in mind that this simple linear approach to the elevation-δ^{18}O relationship does not take into account dynamical effects such as changes in storm tracks and precipitation patterns. Regarding coastal GNIP sites, where instrumental precipitation δ^{18}O records are available (IAEA, Isotope Hydrology Information System: The ISOHIS Database, 2006, accessible at http://isohis.iaea.org) (hereinafter IAEA online data, 2006), the REMO-iso output exhibits a weaker latitudinal gradient (−0.30 ± 0.09‰ per °N) than the GNIP data (−0.73 ± 0.24‰ per °N).

[28] Spatial isotope-temperature slopes are often used as the modern analogue for the temporal slope at the climatic scale when interpreting deep ice core records. However, on a regional scale the isotope signal does not necessarily correspond to the mean surface temperature. Whereas the isotopic composition of precipitation is an integrative parameter that depends on the meteorological conditions along the trajectory from source region to deposition site, surface temperatures are very sensitive to the degree of cloudiness, through clear sky radiative cooling or cloud greenhouse effect, and sea ice coverage for nearby coastal areas. The spatial isotope-temperature slope is a result of physically different mechanisms controlling on one hand the surface temperatures, and on the other hand synoptic conditions and the water isotopes. For Greenland REMO-iso exhibits a δ^{18}O-temperature slope of 0.78 ± 0.01‰/°C, while the observed slope for the combined data from the North Greenland Traverse, ice core sites and Greenland GNIP stations is 0.80 ± 0.03‰/°C. For comparison the spatial slope produced by ECHAM4-iso is 0.71 ± 0.03‰/°C pointing to an underestimation of the depletion of ^{18}O by the coarser resolution global model.

[29] Both the modeled slope of 0.78 ± 0.01‰/°C and the observed slope of 0.80 ± 0.03‰/°C shown in Figure 5c differ from the Greenland slope of 0.67 ± 0.02‰/°C given by *Johnsen et al.* [1989]. However, the slope of 0.67‰/°C was calculated from observations at ice core sites only, and for a much narrower temperature range than the modeled/observed data discussed here.

[30] In order to assess to which degree the bias in the mean temperature over Greenland can explain the bias in the δ^{18}O, we calculated the slope between the anomalies in the modeled δ^{18}O and the anomalies in the modeled temperature. This is done for the Greenland stations and ice core sites in Figure 5a. The result is that the biases in the modeled δ^{18}O and temperature follow a slope of 0.59 ± 0.15‰/°C. There is some scatter in the relation of the anomalies, as indicated by an R^2 of 0.43. The anomalies follow a slightly lower slope than the observed and modeled spatial δ^{18}O-temperature slope, suggesting that the δ^{18}O bias is not solely caused by the bias in temperature, and other less straight forward model biases in δ^{18}O must be at play.

[31] To further investigate the spatial isotope-temperature slope we have calculated local slope by considering the neighboring grid points in a 350 km × 350 km area (Figure 5d). Large differences can be seen across Greenland for the local spatial slope. For example, an area of very steep isotope-temperature slopes near the northeastern and eastern coast of Greenland (see Figure 5c). A similar pattern can be seen in Central Northern Greenland with a relatively rapid change from a steep isotope-temperature gradient west from the center to a flatter gradient east from the center. There is not sufficient observational data to confirm these differences in the regional spatial slope, but the large variability in the spatial slope produced by REMO-iso suggests that the spatial temperature-isotope relation is not straight forward, as also seen in Antarctica [*Masson-Delmotte et al.*, 2008].

3.1.4. The Temporal δ^{18}O-Temperature Slope

[32] In Section 3.1.3 we discussed the δ^{18}O-temperature spatial slope, and mention the application of the spatial slope in connection with reconstruction of past temperatures. However, as past studies have shown, the temporal δ^{18}O-temperature slope is not equal to the spatial δ^{18}O-temperature slope [*Cuffey et al.*, 1992; *Shuman et al.*, 1995, 2001; *Johnsen et al.*, 2001]. In Figure 6 the REMO-iso temporal δ^{18}O-temperature slope for annual mean, monthly mean, JJA mean and DJF mean data are shown. As seen in Figure 6a the slope for the annual mean in the central parts of the ice sheet is between 0.4‰/°C and 0.6‰/°C, which is on the same level as the slope for the monthly means in Figure 6b. For large parts of the ice sheet the annual mean δ^{18}O and temperature are not significantly correlated (non-significant data are masked out), while the pattern for the intra-annual slope on monthly data appears to be correlated with the ice sheet orography (see also Figure 1). The temporal δ^{18}O-temperature slope for JJA is in a similar range as the annual mean slope for the overlapping areas of significant regression, while the DJF slope is generally steeper ranging up to 0.7–1.0‰/°C. This suggests that the low correlations between the summer δ^{18}O and temperature partly offset the steep winter slope within the annual mean correlation. As overlapping time series of observed temperature and δ^{18}O over the Greenland ice sheet are scarce, we are left with comparing the model results to a few case studies of the

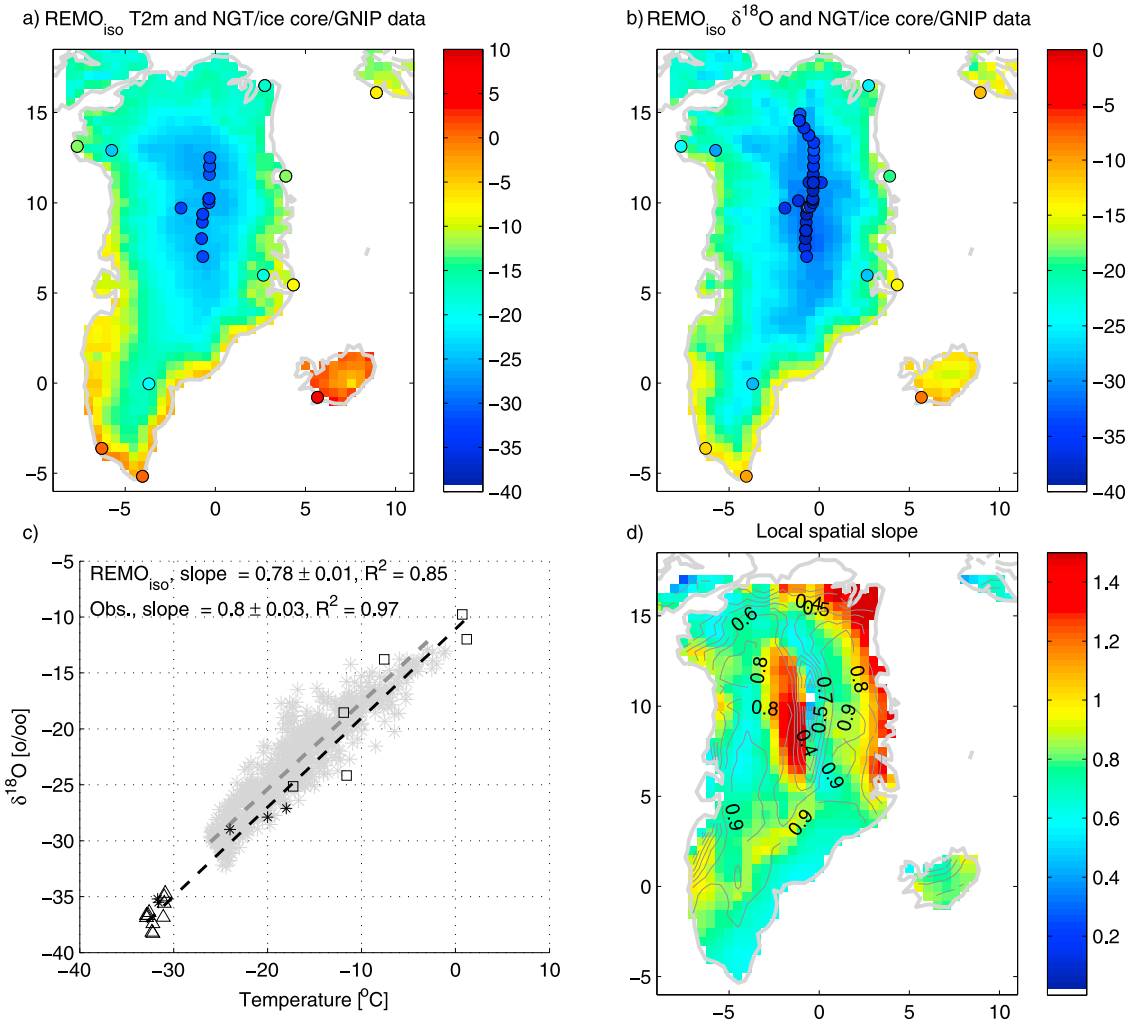

Figure 5. (a) Annual mean REMO-iso temperature (T2m) in °C with observed data from the North Greenland Traverse (where available), ice core sites and GNIP stations. (b) Annual mean modeled δ^{18}O weighted with accumulation in [‰] with observed data from the North Greenland Traverse [*Fischer et al.*, 1998], ice core sites and GNIP stations (IAEA online data, 2006). (c) The spatial regression slope of δ^{18}O versus temperature for Greenland grid points. Model data are the light gray markers, while North Greenland Traverse data are marked with triangles, ice core data with asterisks and GNIP data with squares. The dashed lines are the linear fits for the modeled (gray) and observed (black) data. (d) The local δ^{18}O versus temperature slope calculated for an approximately 350 km × 350 km area in the model grid. Also shown in 0.1 step contours is the R^2 for the same data as the calculated slopes. Data is only shown for $p < 0.05$. ECHAM4-iso counterparts of Figures 5a, 5b and 5c can be found in the auxiliary material (Figure S2).

observed temporal slope. For four ice core sites in the vicinity of the NGRIP and North Greenland Eemian Ice Drilling (NEEM) sites, *Shuman et al.* [2001] reported slopes in the range 0.26–0.31‰/°C for the intra-annual slope, while *Shuman et al.* [1995] gave the value 0.46‰/°C for Summit also for the intra-annual slope. For both these areas REMO-iso exhibits slightly steeper slope values. This could be due to diffusion damping the δ^{18}O annual cycle in the ice core data or REMO-iso overestimating the amplitude of the δ^{18}O annual cycle. For centennial time scales, using the borehole temperature at the GISP2 site near Summit, *Cuffey et al.* [1992] found a slope of 0.53‰/°C, which is in the range of the REMO-iso results for the annual slope close to Summit. Together these results indicate a regionally varying temporal slope, which is generally lower than the spatial δ^{18}O-temperature slope.

3.2. Interannual Variability of Seasonal Data

[33] *Vinther et al.* [2010] demonstrated the fundamentally different behavior of interannual climate variability over Greenland for the summer and winter season. In their publication *Vinther et al.* [2010] put much effort into a proper separation of seasonal isotope signals deduced from different Greenland ice cores. The main findings are that the winter δ^{18}O of Greenland ice cores are strongly correlated with southwest Greenland winter temperature observations and

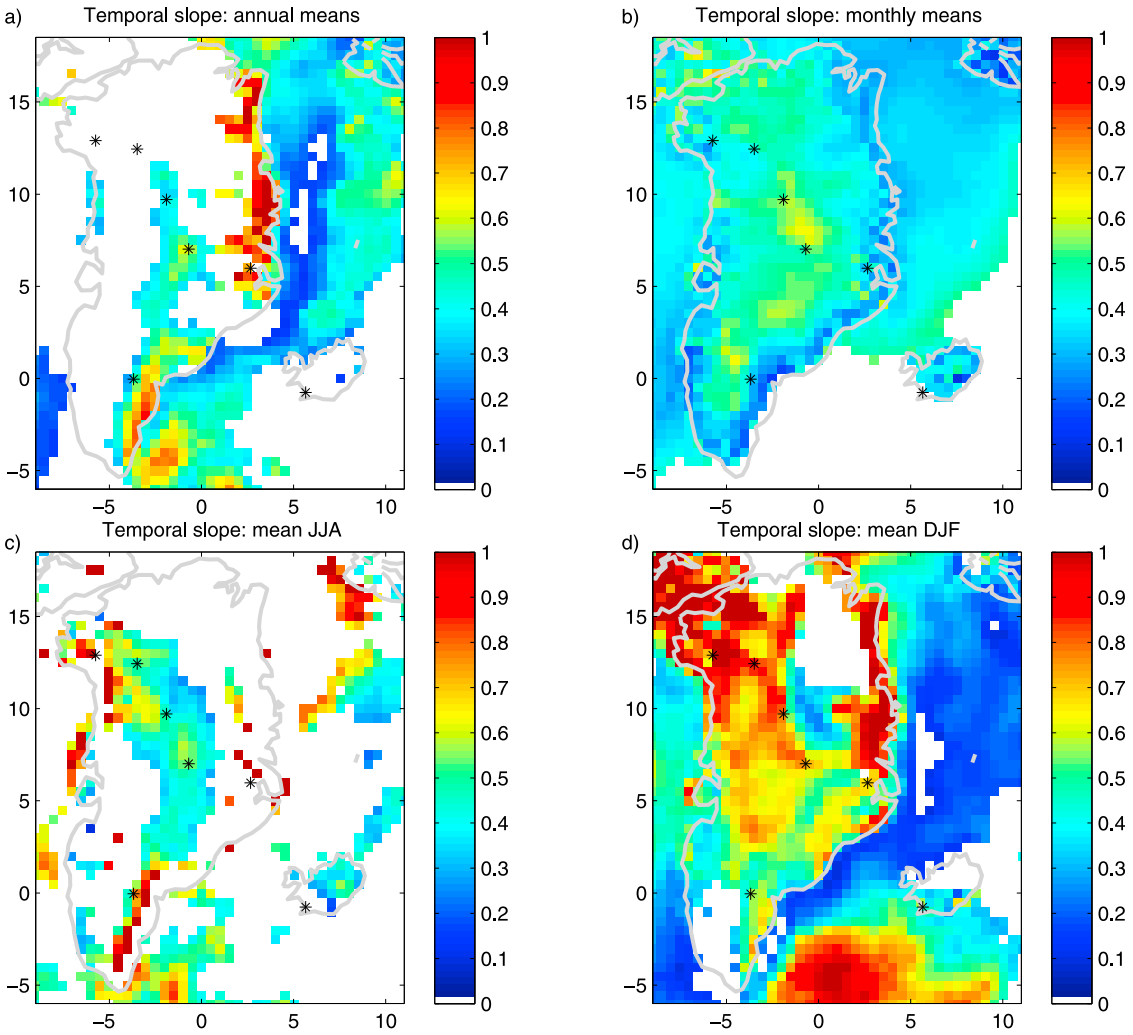

Figure 6. (a) REMO-iso spatial distribution of the temporal slope between $\delta^{18}O$ and T2m [‰/°C] for annual means. Data is only shown for $p < 0.05$. The annual mean $\delta^{18}O$ is accumulation weighted. (b) Same as Figure 6a but for monthly means. (c) Same as Figure 6a but for JJA means with non-weighted $\delta^{18}O$. (d) Same as Figure 6a but for DJF means with non-weighted $\delta^{18}O$.

the NAO circulation pattern, while the summer season $\delta^{18}O$ is associated with summer temperature observations from Stykkisholmur, Iceland, and SSTs around Greenland and Iceland.

[34] In the following, when referring to summer and winter means for modeled, observed and ice core retrieved data, summer is defined as May-October and winter November-April. To explore the effect of accumulation weighting of $\delta^{18}O$ the June-August (JJA), December-February (DJF) and annual means will also be discussed.

3.2.1. Temperature and Precipitation

[35] For this model-data comparison, using the DMI temperature and precipitation data, seasonal means are only calculated when all of the six months are present in the observed data. The common variability between the model data and the observations is calculated here as the square of the linear correlation between the two data sets, thereby giving the percentage of common variability.

[36] Before analyzing the ice core records, the model skill will be estimated by comparing the interannual variability of temperature and precipitation at the coastal weather stations. The results are listed for both REMO-iso and ECHAM4-iso in Table 4. For temperature, the model-data correlation is systematically higher during winter than during summer. Studies of the observed southwest Greenland temperatures show that the winter temperature has more than twice the variability of the summer temperature [*Vinther et al.*, 2006]. The higher winter variability is controlled by large scale circulation features, in particular the NAO [*Hurrell et al.*, 2003].

[37] Since REMO-iso, through the nudging technique, is forced to reproduce the observed circulation patterns, winter temperatures are quite closely matched. For the coastal stations the R^2 between simulated and the observed winter temperature is in the range from 0.47 to 0.85, while the model performs significantly worse during summer with R^2 between 0.01 and 0.69. In summer, local effects poorly constrained by the large scale wind field, such as sea breezes and polar lows, are relatively more important due to the weaker synoptic activity. The model performance for temperature is relatively

Table 4. Interannual R^2 Between Modeled and Observed Seasonal Mean Temperature (T2m) and Precipitation (Pre) for Summer and Winter[a]

Station Number	Name	R^2 REMO-iso T2m Sum/Win	R^2 ECHAM4-iso T2m Sum/Win	R^2 REMO-iso Pre Sum/Win	R^2 ECHAM4-iso Pre Sum/Win
4202	Pituffik	**0.38**/**0.52**[b]	**0.60**/**0.85**[b]	**0.19**[b]/**0.35**[b]	**0.25**[b]/**0.22**[b]
4216	Upernavik	0.01/**0.72**	**0.69**/**0.88**	**0.44**[b]/**0.23**[b]	**0.19**[b]/**0.34**[b]
4220	Aasiaat	**0.15**/**0.63**	**0.78**/**0.86**	**0.27**/**0.19**	**0.52**/**0.35**
4230	Sisimiut	**0.47**[b]/**0.77**[b]	**0.80**[b]/**0.92**[b]	**0.43**[b]/**0.33**[b]	**0.42**[b]/**0.32**[b]
4250	Nuuk	**0.57**/**0.77**	**0.82**/**0.93**	**0.15**/**0.56**	**0.25**/**0.46**
4260	Paamiut	**0.69**/**0.76**	**0.86**/**0.85**	**0.55**/**0.49**[b]	**0.44**/**0.41**[b]
4270	Narsarsuaq	**0.32**/**0.77**	**0.69**/**0.85**	**0.18**/**0.62**	**0.32**/**0.11**
4272	Qaqortoq	**0.54**/**0.85**	**0.78**/**0.87**	**0.22**/**0.31**	**0.34**/0.03
4310	Station Nord	**0.22**[b]/**0.76**[b]	**0.42**[b]/**0.75**[b]	0.09[b]/0.10[b]	**0.51**[b]/**0.53**[b]
4320	Danmarkshavn	**0.24**/**0.64**	**0.45**/**0.79**	0.07/**0.15**	**0.40**/**0.56**
4339	Ittoqqortoormiit	**0.39**/**0.59**	**0.59**/**0.80**	**0.47**/0.02	**0.50**/0.07
4360	Tasiilaq	0.08/**0.54**	**0.50**/**0.74**	**0.13**/**0.37**	**0.63**/**0.25**
4390	Ikerasassuaq	**0.12**[b]/**0.47**[b]	**0.32**[b]/**0.51**[b]	0.09[b]/0.05[b]	**0.24**[b]/**0.24**[b]
-	Reykjavik	**0.68**[b]/**0.84**[b]	0.11[b]/0.04[b]	0.10[b]/**0.49**[b]	0.08[b]/0.10[b]

[a]In the third through fifth columns the first number is R^2 for summer means (Sum) and the second number is R^2 for winter means (Win). Percentages of significant explained variability ($p < 0.05$) are in bold.
[b]There are 5 or more missing values in the seasonally averaged observations.

poor at two western stations, 4216 and 4220, which is due to extremely low SST values in the reanalysis during the first couple of years of the simulation. Local deviations such as this are probably due to a bias in sea ice in ERA-40 for the Greenland fjords. Additionally, there is in the case of station 4360 and 4390 a stronger long-term warming trend in the model output compared to the DMI observations. This is responsible for the low correlation at these two stations.

[38] As expected, the skill of the precipitation simulation is in general worse than for the temperature field (R^2 between 0.02 to 0.61). Overall the simulated interannual precipitation variability is only in slightly better agreement with observations during winter than during the summer season, and does not strictly follow the pattern of model-data coherency found for the temperature variability.

[39] One thing to note with respect to the precipitation observations is the difficulty of collecting samples in Greenland. Even though measures have been taken to improve the procedure of precipitation collection, the strong wind causing blowing snow is still problematic and the precipitation amounts remain unreliable [*Cappelen et al.*, 2001]. The resulting model performance is therefore probably downgraded by the quality of the precipitation data as well.

[40] Comparing the model performance for temperature of the regional and the global model, ECHAM4-iso shows higher R^2 in general than for REMO-iso, in particular during summer (see Table 4). For precipitation the regional and the global model perform on an approximately equal level, with the variability of precipitation of some stations being better reproduced by REMO-iso and the variability of others being better reproduced by ECHAM4-iso. The differences in the nudging schemes for the regional and the global model may explain these differences in model performance. It is however beyond the scope of this study to conclude whether the regional or the global model performs better in terms of variability, as it would require an ensemble run of both models to draw any significance to the differences in correlation with the observations. The fact that REMO-iso and ECHAM4-iso are able to capture a significant fraction of temperature and precipitation variability leads us to expect that these models should be able to capture also part of the observed $\delta^{18}O$ variability.

3.2.2. Isotope Variability

[41] Here the variability of the simulated isotope signal will be evaluated by comparing to observed data from two ice core and three GNIP sites, which have been selected with respect to the quality and temporal range of the observations. The observed isotope data include $\delta^{18}O$ from the Dye-3 and Summit drilling sites, as well as the monthly GNIP observations from Danmarkshavn, Reykjavik and Ny Ålesund. The resolution of both ice cores is sub-annual and allows an evaluation of the modeled$\delta^{18}O$ seasonal variability. Since multiple ice cores have been drilled at both Dye-3 and Summit it is possible to improve the signal to noise ratio of the ice core signal by stacking the individual cores to a single record [*White et al.*, 1997]. The ice core dating is done using numerous tie points, such as volcanic or radioactive markers in addition to annual layer identification, to avoid the propagation of dating errors throughout the entire record. However, the standard deviation for both sites shows a significant spread in the ice core data (see Figures 7 and 8).

[42] As discussed in Section 3.1.3, and evident for the mean annual cycle plotted in Figures 7a and 8a, REMO-iso overestimates the mean $\delta^{18}O$ at both ice core sites. While the model also produces larger seasonal amplitude compared to the ice core data, it should be kept in mind that the Dye-3 ice core data have not been corrected for diffusion. Also, the back-diffusion performed for the Summit ice core data might not recreate the entire amplitude of the original precipitation signal. The very sharp maximum and minimum of summer and winter in the mean annual cycle of the ice core data is a consequence of the peak to peak dating of the data and should be taken as an artifact. The time series of the modeled $\delta^{18}O$ and the ice core data in Figures 7b and 8b give the qualitative impression that REMO-iso produces a realistic $\delta^{18}O$ signal and captures a proportion of the isotopic variability at Dye-3 and Summit. In Table 5 the R^2 between REMO-iso and ECHAM4-iso output and ice core data is listed for the annual mean, seasonal mean, JJA and DJF mean $\delta^{18}O$, as

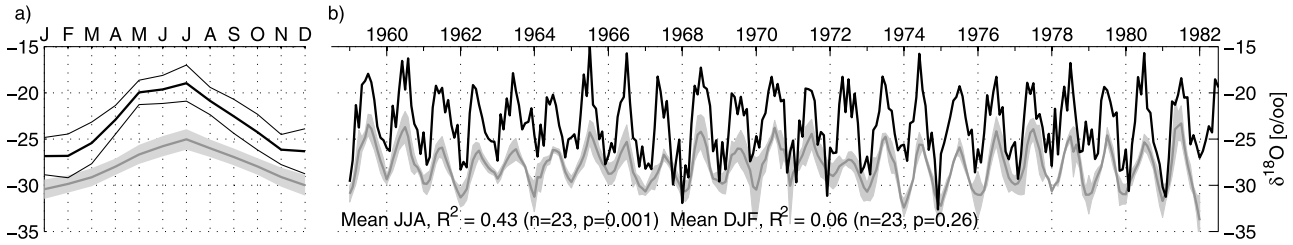

Figure 7. (a) REMO-iso Dye-3 $\delta^{18}O$ annual cycle (black) compared with the stacked ice core mean annual cycle $\delta^{18}O$ values (gray). The thin black lines and the gray shading indicate one standard deviation for model data and ice core data, respectively. (b) Modeled Dye-3 monthly $\delta^{18}O$ (black) compared with stacked ice core data interpolated to monthly values (gray). The light gray shading is the standard deviation between the stacked ice cores. The stacked Dye-3 record consists of four cores, with a minimum of three cores spanning the period shown. The ice core data are dated peak to peak, with the maxima defined as mid July and the minima defined as January. An ECHAM4-iso counterpart of this figure can be found in the auxiliary material (Figure S3).

well at the annual mean accumulation [*Andersen et al.*, 2006]. REMO-iso captures a significant part of the $\delta^{18}O$ variability at Dye-3 for the annual mean and the summer season, while the winter $\delta^{18}O$ of REMO-iso is uncorrelated to the Dye-3 data. For summit REMO-iso fails to capture the variability of the summer season and the annual mean $\delta^{18}O$, while capturing a significant part of the winter variability. The coherency between the modeled (REMO-iso and ECHAM4-iso) $\delta^{18}O$ and the ice core data is very similar for both the accumulation weighted seasonal means and the unweighted JJA/DJF means. Both REMO-iso and ECHAM4-iso capture the variability of the annual mean accumulation well for Summit, with an R^2 of 0.39 and 0.37, respectively, while both models have lower R^2 values for Dye-3. Interestingly, there seem to be no simple connection between the models performance for accumulation and $\delta^{18}O$. For example, at Dye-3 the REMO-iso output is significantly correlated to the ice core $\delta^{18}O$, while not being significantly correlated to the ice core accumulation.

[43] The comparison between ice core data and modeled data is subjected to numerous issues connected to the nature of the ice core data, such as surface processes introducing noise in the ice core records and post depositional diffusion damping the ice core variability [*White et al.*, 1997; *Johnsen*, 1977]. Since the 1960s, precipitation has been collected for isotopic sampling at several weather stations in Greenland. However, the quality of the early data is not always satisfactory and continuous data are not available for most Greenland weather stations. Therefore we here compare the simulated and instrumental isotope signal at three GNIP stations, Ny Ålesund, Reykjavik and Danmarkshavn, with Danmarkshavn being the only Greenland station. All three stations cover the period from the early 1990s till the end of the model run (see also Table 1).

[44] The monthly mean REMO-iso output and observations of $\delta^{18}O$ for the three stations are plotted in Figure 9. The plot of the mean annual cycle of the REMO-iso output and the instrumental $\delta^{18}O$ (Figures 9a, 9c, and 9e) shows an overestimation of the modeled summer $\delta^{18}O$ at all three sites, while the modeled winter level appears to be close to the measured $\delta^{18}O$. There is no bias in the modeled Ny Ålesund and Reykjavik temperature that could explain the offset in the modeled summer $\delta^{18}O$. The summer temperature at Danmarkshavn is overestimated by REMO-iso by about 3°C. In terms of variability, the REMO-iso $\delta^{18}O$ is significantly correlated to the DJF $\delta^{18}O$ of Ny Ålesund ($R^2 = 0.83$) and Danmarkshavn ($R^2 = 0.82$) (see Table 5). At Reykjavik the correlation for $\delta^{18}O$ is relatively low, even though the variability of the temperature for both JJA and DJF means and the mean DJF of precipitation are well reproduced. As REMO-iso, ECHAM4-iso captures a significant part of the DJF $\delta^{18}O$ variability at Ny Ålesund ($R^2 = 0.59$) and Danmarkshavn ($R^2 = 0.50$), but not at Reykjavik.

[45] In summary, the results for the Greenland ice core and GNIP sites show that REMO-iso captures up to 40% of the $\delta^{18}O$ seasonal and interannual variability in the Dye-3

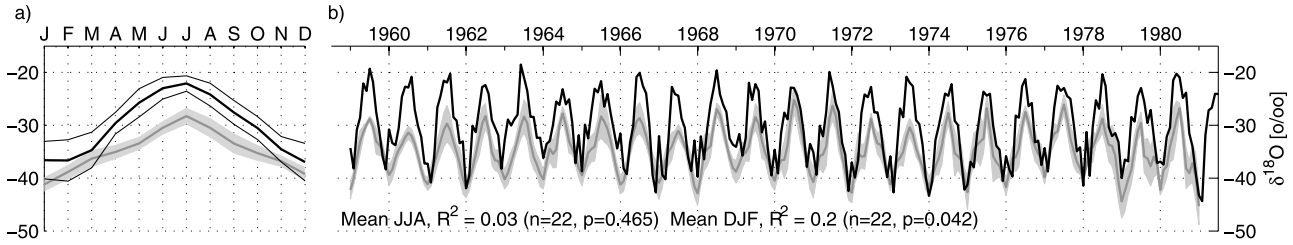

Figure 8. Same as Figure 7 but for Summit. Here the stack is based on six cores, with a minimum of three cores spanning the period shown. The Summit data have been back diffused to partly recreate the original amplitude dampened by post-depositional effects (see also text). An ECHAM4-iso counterpart of this figure can be found in the auxiliary material (Figure S4).

Table 5. Interannual R^2 Between Model Output (REMO-iso and ECHAM4-iso) and Annual Mean $\delta^{18}O$, Accumulation (Acc) and Seasonal Mean $\delta^{18}O$ From the Dye-3 and Summit Ice Cores, as Well as Means for June-July-August (JJA) and December-January-February (DJF) for Interpolated Monthly Ice Core Data[a]

	R^2 Annual $\delta^{18}O$		R^2 Annual Acc		R^2 $\delta^{18}O$ Sum/Win		R^2 $\delta^{18}O$ JJA/DJF	
Site	REMO	ECHAM	REMO	ECHAM	REMO	ECHAM	REMO	ECHAM
Dye-3	**0.40**	0.17	0.13	**0.22**	**0.40**/0.07	**0.26**/**0.19**	**0.43**/0.06	**0.23**/**0.29**
Summit	0.09	**0.34**	**0.39**	**0.37**	0.07/**0.29**	0.15/0.16	0.03/**0.20**	**0.23**/0.15
	R^2 $\delta^{18}O$ JJA/DJF		R^2 T2m JJA/DJF		R^2 pre. JJA/DJF			
	REMO	ECHAM	REMO	ECHAM	REMO	ECHAM		
Ny Ålesund	~0/**0.83**	0.06/**0.59**	**0.45**/**0.56**	0.06/**0.71**	**0.37**/**0.37**	**0.53**/0.01		
Reykjavik	0.10/0.14	0.27/0.27	**0.74**/**0.74**	**0.72**/**0.70**	0.04/**0.52**	0.01/~0		
Danmarkshavn	0.05/**0.82**	0.02/**0.50**	0.20/0.41	0.35/**0.55**	0.05/0.14	0.16/0.32		

[a]The annual mean and seasonal mean model data have been weighted by accumulation, while the JJA and DJF means have not. For the seasonal and JJA/DJF means, the first number of each column is R^2 for summer/JJA means and the second number is R^2 for winter/DJF means. Also listed is R^2 between model output (REMO-iso and ECHAM4-iso) and observed $\delta^{18}O$, T2m and precipitation for the GNIP stations Ny Ålesund, Reykjavik and Danmarkshavn. JJA/DJF means are only included in the correlation analysis if there are no missing data (any month of JJA or DJF) in the instrumental data series. Percentages of significant explained variability ($p < 0.05$) are in bold. The R^2 values listed in this table are valid for the time periods covered in Figures 7, 8 and 9.

and Summit records, while capturing a significant part of the winter variability at Ny Ålesund and Danmarkshavn. For these two GNIP sites the REMO-iso output has higher correlations to the observed $\delta^{18}O$ compared to ECHAM-iso. However, as the GNIP records and the model runs only overlap by 9 to 11 seasons it is a rather short period over which to evaluate the models. As shown for both the ice core and GNIP sites there is no simple connection between the models ability to reproduce the precipitation variability on an annual or seasonal basis, and the models ability to reproduce the $\delta^{18}O$ variability on the same time scales.

3.3. Main Modes of Variability for Temperature, $\delta^{18}O$ and Precipitation

[46] So far we have shown that the nudged simulation with REMO-iso over Greenland has a realistic representation

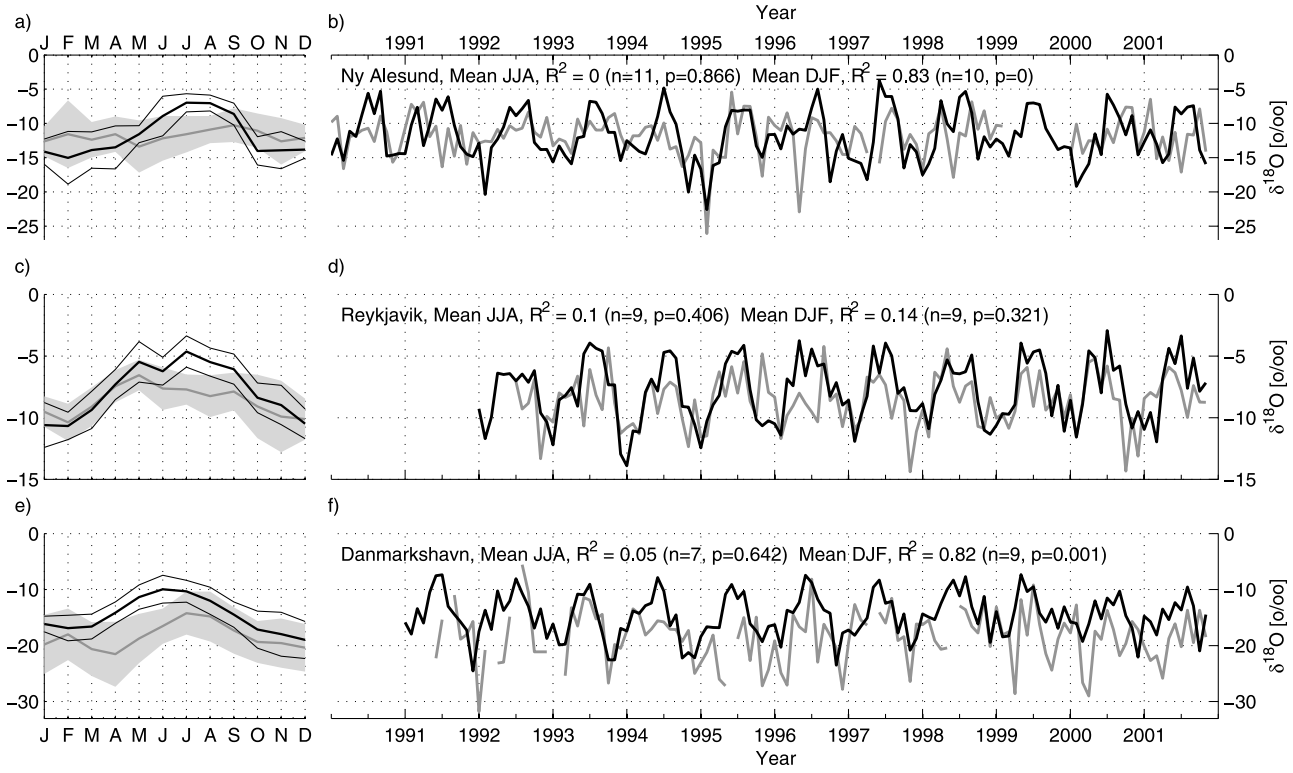

Figure 9. (a) Modeled $\delta^{18}O$ mean annual cycle (black) and measured $\delta^{18}O$ mean annual cycle for Ny Ålesund (gray). The thin black lines and the gray shading indicate one standard deviation for model data and ice core data, respectively. (b) Modeled monthly mean $\delta^{18}O$ (black) and measured monthly mean $\delta^{18}O$ mean annual cycle for Ny Ålesund (gray). (c and d) Same as Figures 9a and 9b but for Reykjavik. (e and f) Same as Figures 9a and 9b but for Danmarkshavn. An ECHAM4-iso counterpart of this figure can be found in the auxiliary material (Figure S5).

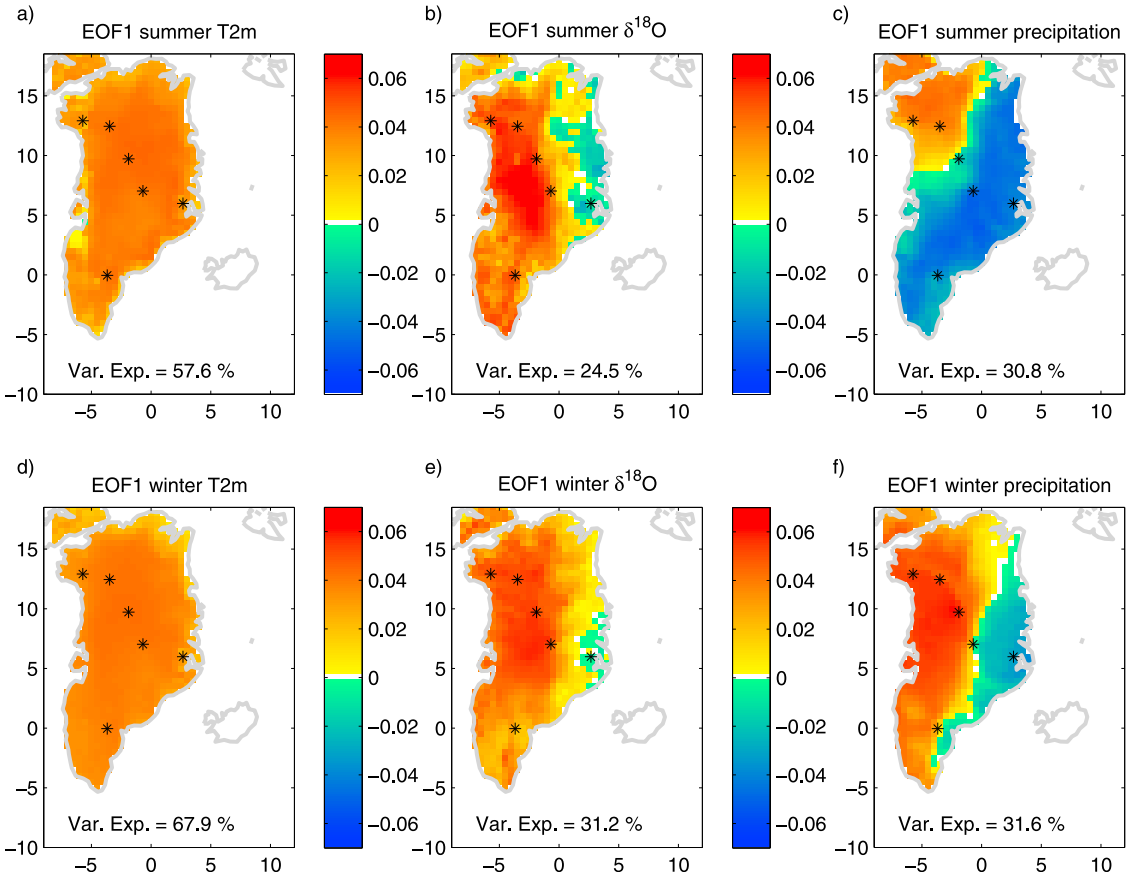

Figure 10. The loadings on PC1 for the seasonal mean temperature, accumulation weighted $\delta^{18}O$ and precipitation for (a, b and c) summer and (d, e and f) winter. The explained variance of the pattern is noted, and the positions of important ice core drilling sites are marked. An ECHAM4-iso counterpart of this figure can be found in the auxiliary material (Figure S6).

of the climatology and variability of meteorological observations, as well as capturing the spatial pattern of $\delta^{18}O$, and a significant part of the $\delta^{18}O$ variability in ice core records at Dye-3 and Summit. While REMO-iso and ECHAM4-iso have similar performances in capturing the observed variability of temperature, precipitation and $\delta^{18}O$, the higher resolution of REMO-iso allows detailed spatial features to be studied. To investigate the spatial coherency of the modeled variability, and to investigate the drivers of the large scale variability, we performed a Principal Component Analysis (PCA) of the REMO-iso seasonal temperature, $\delta^{18}O$ and precipitation. As a part of the PCA procedure the data were centered and normalized. This guarantees that the loadings on the Principal Components (PCs) actually show a true pattern of variability and not only the difference in absolute variability between continental and coastal areas [*Slonosky and Yiou*, 2001]. Here the common practice of using the term Empirical Orthogonal Functions (EOFs) for the spatial patterns of the loadings on the PCs, and using the term PCs for the time series of the PCs is adopted. Using the "rule of thumb" suggested by *North et al.* [1982], only the eigenvalues of the first EOFs have been found not to be possibly *effectively degenerated* for all three variables: temperature, $\delta^{18}O$ and precipitation.

[47] As also mentioned in Section 1.1 the importance of the NAO for the Greenland climate variability has been shown in several studies. Iceland is at one of the centers of action of the NAO, and for the period 1959–2001 the modeled pressure variations at Reykjavik are in close agreement with the observed ones (winter $R^2 = 0.77$, summer $R^2 = 0.70$). The general and well-known impact of the NAO is a varying strength of the meridional versus zonal circulation over the North Atlantic. As a consequence, colder (NAO positive) and warmer (NAO negative) temperatures are encountered in Greenland, with the opposite being true for Western Europe [*Hurrell et al.*, 2003].

3.3.1. The Loading on the First Principal Components

[48] In the following we will focus on EOF1 of temperature, $\delta^{18}O$ and precipitation. The explained variability of EOF1 of each of the three variables is systematically lower for the summer means than for the winter means. For temperature the first EOF explains more than 50% of the interannual variability (58% and 68% for summer and winter respectively), whereas both precipitation and the $\delta^{18}O$ pattern explain a comparable fraction of the total variability of about 20–30% (see also Figure 10). The winter and summer EOFs for temperature are uniform over all of Greenland, with the exception of relatively weak loadings on the eastern coast of

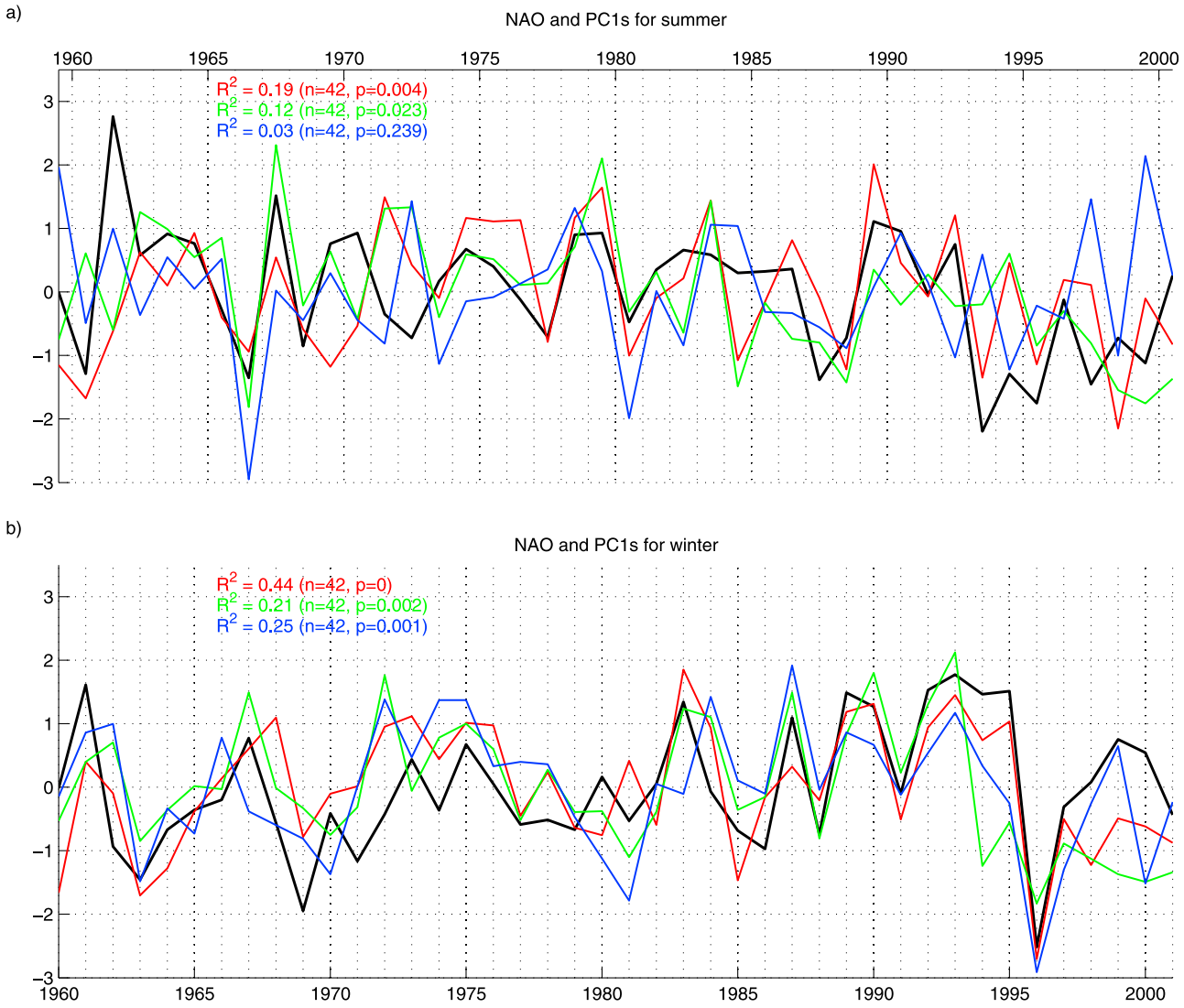

Figure 11. (a) Time series of the first PC of mean summer temperature (red), accumulation weighted $\delta^{18}O$ (green) and precipitation (blue), as well as the observed mean summer NAO (black). (b) Same as Figure 11a but for winter. The R^2 between each of the PCs and the NAO is listed in matching colors.

Greenland, while EOF1 for precipitation has a strong dipole structure over Greenland in winter, and the summer EOF1 for precipitation has a structure more oriented towards a northwest-southeast pattern. The maximum winter loadings on PC1 for precipitation in the western part of Greenland include NGRIP, Camp Century, and the new NEEM deep drilling sites. The EOF1 for winter $\delta^{18}O$ resembles EOF1 of the winter temperature with the exception of the eastern part of Greenland, where the loadings are weak or negative. The simulated EOF1 of $\delta^{18}O$ (summer and winter) next to the ice core drilling site Renland for instance (see Figures 10b and 10e), has little common variability with the central Greenland sites such as Summit and NGRIP. This loss of common variability between Renland and the Central Greenland isotope records is supported by a PCA study of Greenland ice core data [*Vinther et al.*, 2010]. The weak loadings for the $\delta^{18}O$ pattern is an effect of precipitation weighting of the isotope signal on a sub-seasonal time-scale.

3.3.2. Relation to the NAO

[49] The link between the EOFs of the REMO-iso output and the NAO is illustrated in Figure 11, where the times series of the first PCs and the NAO are shown. Furthermore, an 11-year running correlation between the first PCs and the NAO is calculated. The 11-year running correlation allows for variations in the strength of the correlation to be picked up within the 43-year model run, and the significance of the running correlation is estimated via a bootstrap algorithm (see the caption of Figure 12 for details). A significant negative correlation is seen in Figure 12 for PC1 of the winter temperature for the full period, with only a brief interval of weaker correlation during the 1970s. For the period from 1959 to 2001, the temperature PC1 correlation with the NAO is significantly higher in winter ($R^2 = 0.44$) than in summer ($R^2 = 0.19$). This is in line with the studies of *Slonosky and Yiou* [2001]; *Vinther et al.* [2003] that show the impact of the NAO on winter temperature variability in the entire circum North Atlantic region. The running correlation in

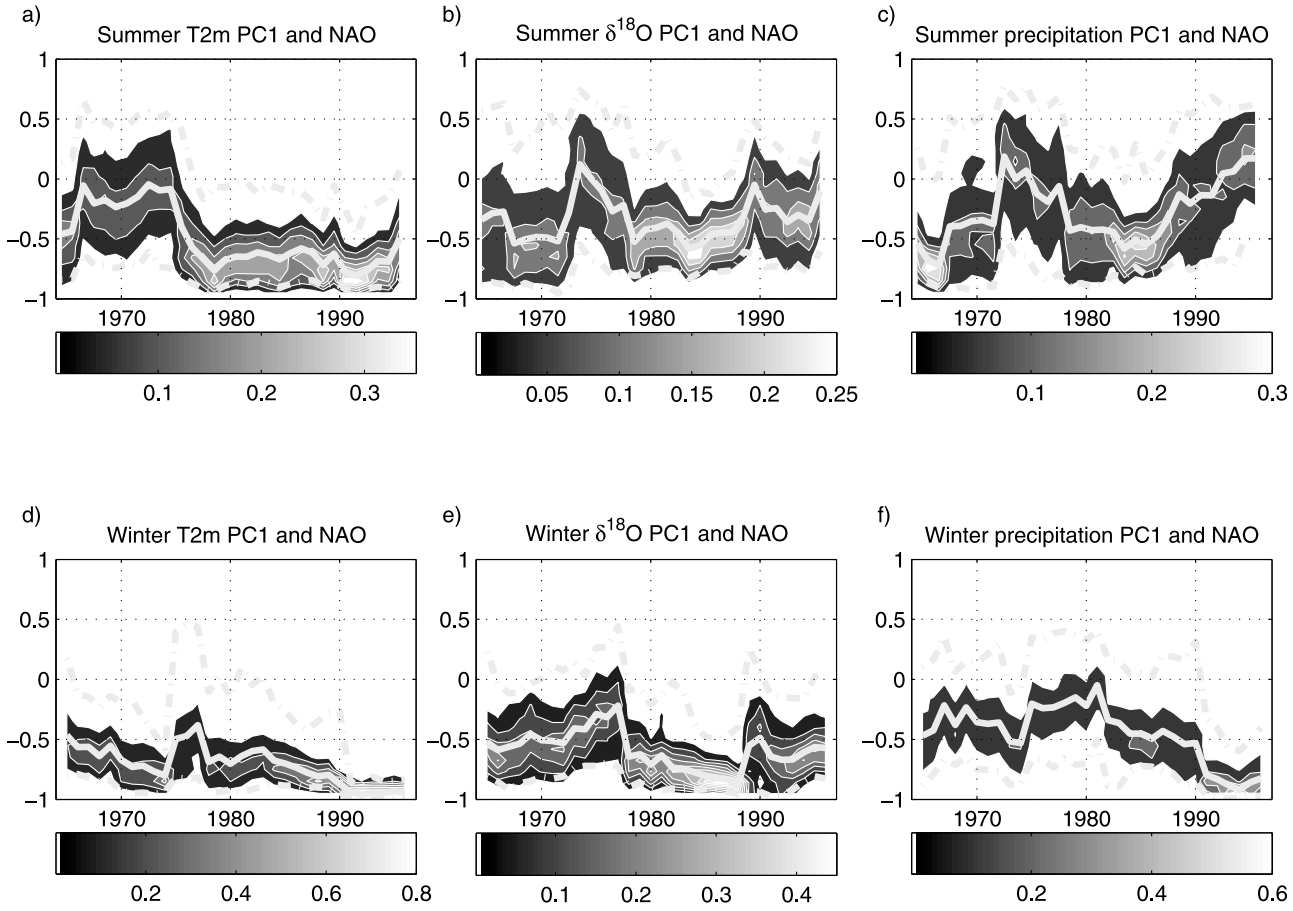

Figure 12. The 11 year running correlation (full gray line) between the seasonal mean NAO and the first PCs of seasonal temperature, accumulation weighted δ^{18}O and precipitation for (a, b and c) summer and (d, e and f) winter. The significance of the correlation is estimated using bootstrap re-sampling [*Efron*, 1983] with 1000 samples for each collection of 11 data pairs. The bootstrap method is re-sampling with replacement for random selections from the sample. With bootstrap re-sampling the statistical properties of a sample can be calculated empirically, without making assumptions about the nature of the statistical distribution. The contour shades give the density of the bootstrap correlation with the colorbar indicating the percentage of bootstrap correlations marked by the colors. Marked with the dash-dotted gray lines is the upper and lover limits of the 95% confidence intervals also calculated using the bootstrap method. An ECHAM4-iso counterpart of this figure can be found in the auxiliary material (Figure S7).

Figure 12 between the PC1 of winter precipitation and NAO shows that the correlation is negative for the full period, but only periodically significant with a marked shift to strongly significant negative correlation during the 1990s. As for the case of temperature and precipitation the winter PC1 of δ^{18}O is negatively correlated with NAO during the whole model run (see Figure 12e). The shift in correlation for δ^{18}O towards more negative values in the second half of the 1970s coincides with the shift for the temperature PC1 ending the brief period of weak correlations.

[50] Except for this shift, the PC1 of temperature, δ^{18}O and precipitation have little in common in terms of temporal changes in the running correlation with the NAO. The weak correlations during the second half of the 1970s could be a consequence of the low amplitude of the NAO in the same period (see Figure 11). *Vinther et al.* [2003] found the correlation between the PC1 of δ^{18}O of seven Greenland ice cores and the NAO to vary in strength and significance over the past ~400 years. The time variation in the correlation between the δ^{18}O and the NAO, found both in this study and in work by *Vinther et al.* [2003], points to the NAO mode being less dominant in certain time intervals. This is also in agreement with the accumulation study by *Appenzeller et al.* [1998] in western Greenland, where it was suggested that the NAO is an intermittent climate oscillation with active and passive phases. The explained variance of the PCA and the correlation between the NAO and the PCs is summarized in Table 6. As well as being correlated to the NAO the first PCs of temperature, δ^{18}O and precipitation are positively correlated to each other ($R^2 \sim 0.5$).

[51] To summarize the influence of the NAO in the REMO-iso simulation: for the negative phase NAO Greenland enters a warm mode with a dipole precipitation pattern of more precipitation in the west and less precipitation in the east, while for the positive NAO phase Greenland enters a cold mode with a dipole precipitation pattern of less precipitation

Table 6. Explained Variance of the First Two EOFs for Mean Seasonal Temperature, $\delta^{18}O$ and Precipitation, and Common Variance (R^2) of the First Two PCs of the Modeled Data With the Seasonally Averaged NAO[a]

	Explained Variance		R^2 With NAO $p < 0.05$	
	Summer (May-Oct)	Winter (Nov-Apr)	Summer (May-Oct)	Winter (Nov-Apr)
		T2m		
EOF1	0.58	0.68	**0.19**	**0.44**
EOF2	0.13	0.12	0.02	0.03
		$\delta^{18}O$		
EOF1	0.24	0.31	**0.12**	**0.21**
EOF2	0.11	0.15	~0	~0
		Precipitation		
EOF1	0.31	0.32	0.03	**0.25**
EOF2	0.19	0.22	**0.10**	0.01

[a]Percentages of significant explained variability ($p < 0.05$) are in bold.

in the west and more precipitation in the east. Influenced by the same circulation patterns as temperature and precipitation, the $\delta^{18}O$ shows an integrated climate signal with traits of both the temperature and precipitation EOF pattern.

[52] As supplement to the PCA we have calculated the point-wise regression of temperature, $\delta^{18}O$ and precipitation with the NAO, and the results for temperature and precipitation are compared with the correlation between the NAO and the coastal observations by DMI (see Figure 13). These results confirm the important role of the NAO for the considered climate variables, and give additional confidence in the model's capacity to reproduce the influence of the circulation on temperature, $\delta^{18}O$ and precipitation. First, there are similarities in the correlation pattern in Figure 13 and the corresponding PC1 (Figure 10), especially for temperature. This is of course to be expected since in particular the NAO related temperature PC1 explains a very large part of the interannual variability (see Figures 10d and 12d). Secondly, the comparison with the meteorological data (colored dots in Figure 13) gives strong empirical support for the computed NAO correlation pattern. While the correlation pattern between winter $\delta^{18}O$ and NAO has similarities to the first EOF of $\delta^{18}O$ the correlations are only significant in central and southeastern Greenland. This could be related to the lack of winter accumulation in northwestern Greenland (see Figure 3d). For the northwestern area with low winter accumulation the standard deviation of the mean winter $\delta^{18}O$ is twice as high as for southern Greenland (not shown),

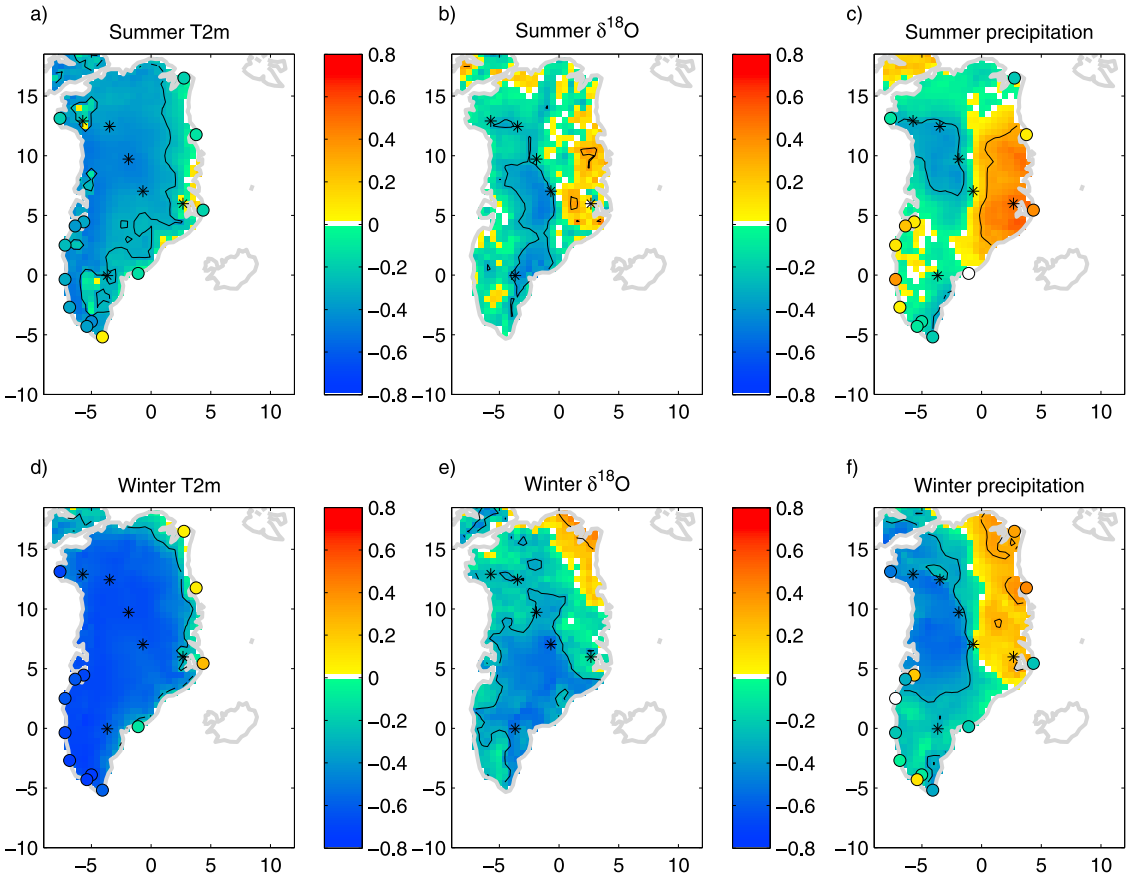

Figure 13. Point-wise correlation maps between the seasonal mean observed NAO and the modeled (a, b and c) summer and (d, e and f) winter temperature, accumulation weighted $\delta^{18}O$ and precipitation, with the contour line (black) marking $p = 0.05$. The colored dots in the temperature and precipitation maps indicate the correlation between observations and the seasonal mean NAO. An ECHAM4-iso counterpart of this figure can be found in the auxiliary material (Figure S8).

signifying more noise in the winter signal. This could reduce the correlation of the $\delta^{18}O$ to the NAO.

[53] From the EOFs and correlation patterns with the NAO, it is possible to point out areas of the Greenland ice sheet that are sensitive to NAO variability. In terms of precipitation, central western Greenland (west of Summit) is both within the area of high loadings on the first PC as well as being significantly correlated with the NAO. This area is also the focus of accumulation-NAO study of *Appenzeller et al.* [1998]. For a pure NAO signal in $\delta^{18}O$ it would be preferable not to have a signal also modulated by precipitation. The Summit area close to the Greenland Ice core Project (GRIP) ice core site has low correlations between the precipitation and NAO, and is also located at the saddle point of the precipitation seesaw related to the NAO. The winter signal can be expected to be intact as the area has about 40% of winter precipitation, and both the loadings on the first PC for $\delta^{18}O$ and the correlation of the $\delta^{18}O$ with the NAO. Estimated from the REMO-iso output, the Summit area should be the most liable candidate for a strong NAO signal in the $\delta^{18}O$. This is also supported by studies of the Greenland Ice Sheet Project 2 (GISP2) ice core near Summit [*Barlow et al.*, 1997; *White et al.*, 1997]. It is possible that a composite of high resolution records of accumulation from western central Greenland and $\delta^{18}O$ from Summit would aid to reconstruct the circulation patterns over the North Atlantic region.

4. Discussion and Conclusion

[54] This study evaluates the REMO-iso regional climate model over Greenland in comparison with observations and ice core data, and investigates the main variability patterns for temperature, $\delta^{18}O$ and precipitation in relation to the NAO. The climatological mean spatial distribution and annual cycles of temperature, precipitation and $\delta^{18}O$ are well reproduced. The evaluation also shows the benefits of the high spatial resolution of REMO-iso compared to ECHAM4-iso in reproducing the spatial temperature-$\delta^{18}O$ slope and the absolute values of $\delta^{18}O$ over the ice sheet, as well as resolving features on a local scale not possible for course resolution models. In terms of variability REMO-iso and ECHAM4-iso exhibit similar skill in reproducing the observed temperature, $\delta^{18}O$ and precipitation from meteorological stations and ice core sites, although ECHAM4-iso generally has better skill in reproducing the temperature variability. Due to differences in the nudging scheme of REMO-iso and ECHAM4-iso, REMO-iso is more loosely constrained in relation to the ERA-40 reanalysis. It would be desirable for future experiments to use an ensemble approach or possibly employing an ensemble of nudged regional model runs. This could maximize the coherency between the model and the observations, and give an estimate of the spread of the model output.

[55] Of three GNIP stations, the REMO-iso and ECHAM4-iso output is correlated significantly to the winter $\delta^{18}O$ of Ny Ålesund and Danmarkshavn, with REMO-iso having higher correlations than ECHAM4-iso. However, these data series are comparably short (~10 years) with some months missing. REMO-iso captures a significant part of the interannual $\delta^{18}O$ variability of the Dye-3 and Summit ice cores. However, the model fails to capture some aspects of the seasonal and annual variability, which could be related to the difficulties of a direct comparison between the gridded model output and the local ice core data. The available ice core records only span ~20 years of the simulation, and multiple ice cores covering the full model run would be optimal for evaluating the variability of the model output. Additionally, this model study only extends to 2001. With the recent reanalysis product of the ECMWF, ERA-Interim the model run could be extended until present [*Dee et al.*, 2011]. Both GNIP and ice core data (e.g. the NEEM ice core) are available for after 2001 for extending the model evaluation, and shed light on recent developments in climate.

[56] As summarized above, REMO-iso shows considerable skill over Greenland, there are however significant biases of which the most pronounced are listed below.

[57] 1. For inland Greenland there is a bias for mean annual temperature of about +5°C. The bias is stronger towards the north, and for both southern and northern regions strongest during summer.

[58] 2. In the northern central Greenland the accumulation is underestimated by about 25%.

[59] 3. Compared to ice core data there is a bias in annual mean $\delta^{18}O$ of +4.4‰. Seasonally, this bias is also strongest during summer.

[60] It is likely that the temperature bias can be explained by too low surface albedo in REMO-iso, causing too warm temperatures especially during summer. The dry bias in central Greenland could be related too low resolution. Even the ~55 km used in this study could be too coarse to achieve realistic vapor transport to very cold regions. With respect to $\delta^{18}O$, the slope of the annual mean $\delta^{18}O$ and temperature biases, as well as the seasonality of the $\delta^{18}O$ and temperature biases, suggests that at least part of the $\delta^{18}O$ bias can be explained by too high temperatures. However, the northward depletion of ^{18}O and the temperature-$\delta^{18}O$ slope is in fact also underestimated, which means that the $\delta^{18}O$ bias is not only caused by temperature. In the GCM study by *Masson-Delmotte et al.* [2008], the models were also fitted with isotope diagnostics. The authors reported a positive Antarctic bias in δD, which they attributed to a cold regions dry bias. A dry bias for cold regions means that there will be even less snow during cold periods, creating a precipitation weighting towards more positive mean $\delta^{18}O$ values. With the REMO-iso dry bias in mind, this and the temperature bias could explain the overestimated $\delta^{18}O$ values for inland Greenland. However, a study on short time scales resolving individual precipitation events or a simulation with higher horizontal resolution is necessary to quantify this.

[61] The analysis of the main modes of variability shows that the first PCs of the mean winter temperature, $\delta^{18}O$ and precipitation are all correlated to the NAO. The significance of the spatial structure of the EOFs is emphasized by the correlation between the NAO and observed temperature and precipitation. Based on this we suggest that the NAO could be reconstructed using a combination of accumulation and $\delta^{18}O$ records from ice cores, with the ice core sites being picked with consideration to where the correlation to the NAO is strongest and most stable. For the $\delta^{18}O$ record, a site with little correlation between accumulation and NAO should be chosen to avoid that the $\delta^{18}O$ signal is modulated by changes accumulation amounts. Our recommendation is that $\delta^{18}O$ records from the summit region and an accumulations record from western central Greenland are chosen for future NAO

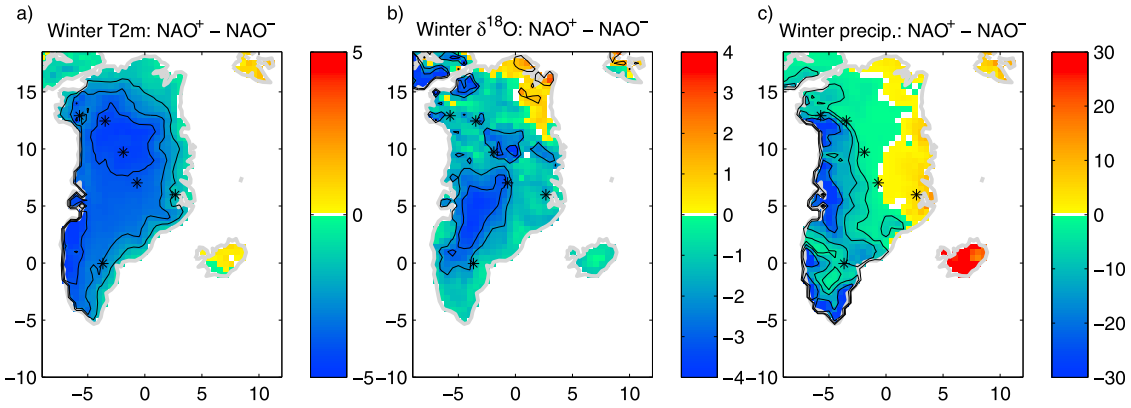

Figure 14. Difference between the 5 winters with the highest NAO index and the 5 winters with lowest NAO index, for REMO-iso mean winter (a) T2m [°C], (b) δ^{18}O [‰] and (c) precipitation [mm/month] for the period 1960–2000. Contour lines are plotted for −4, −3 and −1°C (Figure 14a, −3, −2 and −1‰ (Figure 14b) and −20, −10 and −5 mm/month (Figure 14c).

reconstructions. However, as pointed out by this and other studies, the influence of the NAO is not static in time. This is an issue if the reconstruction method is only considering the NAO, and not circulation regimes in a broader sense.

[62] *Sodemann et al.* [2008] recommended using sites south of 65°N, at the southern dome of the ice sheet, and on the central eastern plateau for reconstructing the NAO from δ^{18}O. This was based on 30 selected winter months of the ERA-40 reanalysis, that formed the basis of the Lagrangian method of *Sodemann et al.* [2008]. These recommendations differ from what is suggested in this study. A direct comparison between the two studies is prevented by differences in the methods and data analysis. Nevertheless, the apparent difference in the sensitivity of δ^{18}O to the NAO is interesting, since both this study and the study by *Sodemann et al.* [2008] use the ERA-40 as forcing. The use of seasonal data in this study, as opposed to monthly data of *Sodemann et al.* [2008], can probably partly explain this difference. We would like to stress that model predictions of climate signals in ice cores data should be given in terms of what can be retrieved from ice cores. Given the uncertainties in the ice core dating, and the seasonal ice core study by *Vinther et al.* [2010], seasonal resolution is the highest resolution that can be expected to be retrieved. This is also the motivation for the separation of the model data in two seasons for this study. To estimate the absolute amplitude of the impact of the NAO, the difference between the mean winter T2m, δ^{18}O and precipitation of the 5 winters with the highest NAO index and the 5 winters with lowest NAO index is shown in Figure 14. The maps in Figure 14 resemble the correlation maps between NAO and winter T2m, δ^{18}O and precipitation (Figures 13d, 13e and 13f). For δ^{18}O, the result is ∼−3‰ difference for the Summit region. However, the standard deviation (not shown) is of the same magnitude. This is comparable to the estimate of *Sodemann et al.* [2008] (3.8 ± 6.8‰) for the difference between NAO^- and NAO^+ situations. For the central western Greenland, the impact of the NAO amounts to 5–10 mm/month (Figure 14b). This gives 50 mm on a seasonal scale.

[63] This first regional modeling study of the δ^{18}O in Greenland precipitation points out the strengths and limitations of our current modeling abilities. As shown in the model evaluation of REMO-iso, the high spatial resolution allows for more realistic ice sheet orography that is very important for realistic representation of the δ^{18}O. This makes REMO-iso particularly useful for sensitivity studies of the ice sheet elevation for the past climate, where the ice sheet orography was different [*Otto-Bliesner et al.*, 2006; *Vinther et al.*, 2009]. Additionally we have pointed out the scarcity of available high resolution instrumental δ^{18}O and ice core data to evaluate studies such as this. To further test the REMO-iso model framework, and similar isotope models, new data must be made available. This includes isotopic data on an event-based resolution from both vapor and precipitation [*Steen-Larsen et al.*, 2011], as well as multiple high resolution ice core for improved signal to noise ratio. With the recent advances in the use of laser spectroscopy for vapor and water samples a high resolution isotopic sampling network is within reach [*Gkinis et al.*, 2010; *Iannone et al.*, 2010; *Gupta et al.*, 2009]. Since the REMO-iso model framework is capable of calculating the actual weather patterns, such a sampling network would allow for an evaluation of the model at the time scale of synoptic systems.

[64] The approach suggested above would aid both the evaluation of the modeling of stable isotopes and the understanding of the physics behind the high frequency isotope variability and the nature of the isotopic climate proxies.

[65] **Acknowledgments.** This research was funded by the Danish Agency for Science, Technology and Innovation, the Niels Bohr Institute, University of Copenhagen, CEA-CNRS and Agence Nationale de la Recherche (ANR NEEM and ANR CEPS GREENLAND grants). The model experiments were carried out at the German Climate Computing Centre (DKRZ), Hamburg. The authors thank three anonymous reviewers for helpful comments and suggestions.

References

Andersen, K. K., P. D. Ditlevsen, S. O. Rasmussen, H. B. Clausen, B. M. Vinther, S. J. Johnsen, and J. P. Steffensen (2006), Retrieving a common accumulation record from Greenland ice cores for the past 1800 years, *J. Geophys. Res.*, *111*, D15106, doi:10.1029/2005JD006765.

Appenzeller, C., T. Stocker, and M. Anklin (1998), North Atlantic oscillation dynamics recorded in Greenland ice cores, *Science*, *282*(5388), 446–449.

Bales, R., J. McConnell, E. Mosley-Thompson, and G. Lamorey (2001), Accumulation map for the Greenland Ice Sheet: 1971–1990, *Geophys. Res. Lett.*, *28*(15), 2967–2970, doi:10.1029/2000GL012052.

Bales, R. C., Q. Guo, D. Shen, J. R. McConnell, G. Du, J. F. Burkhart, V. B. Spikes, E. Hanna, and J. Cappelen (2009), Annual accumulation for Greenland updated using ice core data developed during 2000–2006 and analysis of daily coastal meteorological data, *J. Geophys. Res.*, *114*, D06116, doi:10.1029/2008JD011208.

Barlow, L., J. Rogers, M. Serreze, and R. Barry (1997), Aspects of climate variability in the North Atlantic sector: Discussion and relation to the Greenland Ice Sheet Project 2 high-resolution isotopic signal, *J. Geophys. Res.*, *102*(C12), 26,333–26,344, doi:10.1029/96JC02401.

Box, J., and A. Rinke (2003), Evaluation of Greenland ice sheet surface climate in the HIRHAM regional climate model using automatic weather station data, *J. Clim.*, *16*(9), 1302–1319.

Box, J. E., D. H. Bromwich, B. A. Veenhuis, L.-S. Bai, J. C. Stroeve, J. C. Rogers, K. Steffen, T. Haran, and S.-H. Wang (2006), Greenland ice sheet surface mass balance variability (1988–2004) from calibrated polar MM5 output, *J. Clim.*, *19*(12), 2783–2800, doi:10.1175/JCLI3738.1.

Bromwich, D., and S. Wang (2005), Evaluation of the NCEP-NCAR and ECMWF 15- and 40-Yr Reanalyses using rawinsonde data from two independent Arctic field experiments, *Mon. Weather Rev.*, *133*(12), 3562–3578.

Bromwich, D. H., R. L. Fogt, K. I. Hodges, and J. E. Walsh (2007), A tropospheric assessment of the ERA-40, NCEP, and JRA-25 global reanalyses in the polar regions, *J. Geophys. Res.*, *112*, D10111, doi:10.1029/2006JD007859.

Cappelen, J., B. Joergensen, E. Laursen, L. Stannius, and R. Thomsen (2001), The observed climate of Greenland, 1958–99 - with climatological standard normals, 1961–90, *Tech. Rep. 00-18*, Dan. Meteorol. Inst., Copenhagen.

Church, J. A., J. M. Gregory, P. Huybrechts, M. Kuhn, K. Lambeck, M. T. Nhuan, D. Qin, and P. L. Woodworth (2001), Changes in sea level, in *Climate Change 2001: The Scientific Basis. Contribution of Working Group I to the Third Assessment Report of the Intergovernmental Panel on Climate Change*, chap. 11, p. 651, Cambridge Univ. Press, Cambridge, U. K.

Ciais, P., and J. Jouzel (1994), Deuterium and oxygen-18 in precipitation: Isotopic model, including mixed cloud processes, *J. Geophys. Res.*, *99*(D8), 16,793–16,803.

Cuffey, K., R. Alley, P. Grootes, and S. Anandakrishnan (1992), Toward using borehole temperatures to calibrate an isotopic paleothermometer in central Greenland, *Global Planet. Change*, *98*(2-4), 265–268.

Dansgaard, W. (1953), The abundance of ^{18}O in atmospheric water and water vapor, *Tellus*, *5*(4), 461–469, doi:10.1111/j.2153-3490.1953.tb01076.x.

Dee, D. P., et al. (2011), The ERA-Interim reanalysis: Configuration and performance of the data assimilation system, *Q. J. R. Meteorol. Soc.*, *137*(656), 553–597, doi:10.1002/qj.828.

Efron, B. (1983), The Jackknife, the Bootstrap and other resampling plans, *J. Am. Stat. Assoc.*, *78*(384), 987–1001.

Fischer, H., M. Werner, D. Wagenbach, M. Schwager, T. Thorsteinnson, F. Wilhelms, J. Kipfstuhl, and S. Sommer (1998), Little Ice Age clearly recorded in northern Greenland ice cores, *Geophys. Res. Lett.*, *25*(10), 1749–1752, doi:10.1029/98GL01177.

Gkinis, V., T. J. Popp, S. J. Johnsen, and T. Blunier (2010), A continuous stream flash evaporator for the calibration of an IR cavity ring down spectrometer for isotopic analysis of water, *Isotopes Environ. Health Stud.*, *46*, 463–475.

Gupta, P., D. Noone, J. Galewsky, C. Sweeney, and B. H. Vaughn (2009), Demonstration of high-precision continuous measurements of water vapor isotopologues in laboratory and remote field deployments using wavelength-scanned cavity ring-down spectroscopy (WS-CRDS) technology, *Rapid Commun. Mass Spectrom.*, *23*(16), 2534–2542, doi:10.1002/rcm.4100.

Herold, M., and G. Lohmann (2009), Eemian tropical and subtropical African moisture transport: An isotope modelling study, *Clim. Dyn.*, *33*(7-8), 1075–1088, doi:10.1007/s00382-008-0515-2.

Hoffmann, G., and M. Heimann (1997), Water isotope modeling in the Asian monsoon region, *Quat. Int.*, *37*, 115–128.

Hoffmann, G., M. Werner, and M. Heimann (1998), Water isotope module of the ECHAM atmospheric general circulation model: A study on timescales from days to several years, *J. Geophys. Res.*, *103*(D14), 16,871–16,896.

Hurrell, J. W., Y. Kushnir, G. Ottersen, and M. Visbeck (2003), An overview of the North Atlantic Oscillation, in *The North Atlantic Oscillation: Climatic Significance and Environmental Impact*, *Geophys. Monogr. Ser.*, vol. 134, edited by J. W. Hurrell et al., pp. 1–35, AGU, Washington, D. C., doi:10.1029/134GM01.

Iannone, R. Q., D. Romanini, O. Cattani, H. A. J. Meijer, and E. R. T. Kerstel (2010), Water isotope ratio (δ^2H and $\delta^{18}O$) measurements in atmospheric moisture using an optical feedback cavity enhanced absorption laser spectrometer, *J. Geophys. Res.*, *115*, D10111, doi:10.1029/2009JD012895.

Jacob, D. (2001), A note to the simulation of the annual and inter-annual variability of the water budget over the Baltic Sea drainage basin, *Meteorol. Atmos. Phys.*, *77*(1-4), 61–73.

Jacob, D., and R. Podzun (1997), Sensitivity studies with the regional climate model REMO, *Meteorol. Atmos. Phys.*, *63*(1-2), 119–129.

Jeuken, A., P. Siegmund, L. Heijboer, J. Feichter, and L. Bengtsson (1996), On the potential of assimilating meteorological analyses in a global climate model for the purpose of model validation, *J. Geophys. Res.*, *101*(D12), 16,939–16,950.

Joergensen, P., and E. Laursen (2003), DMI Monthly Climate Data Collection 1860–2002, Denmark, Faroe Island and Greenland, *Tech. Rep. 03-26*, Dan. Meteorol. Inst., Copenhagen.

Johnsen, S. (1977), Stable isotope homogenization of polar firn and ice, *IAHS-AISH Publ.*, *118*, 210–219.

Johnsen, S., W. Dansgaard, and J. White (1989), The origin of arctic precipitation under present and glacial conditions, *Tellus, Ser. B*, *41*, 452–468, doi:10.1111/j.1600-0889.1989.tb00321.x.

Johnsen, S. J., et al. (1992), Irregular glacial interstadials recorded in a new Greenland ice core, *Nature*, *359*(6393), 311–313, doi:10.1038/359311a0.

Johnsen, S., D. Dahl-Jensen, N. Gundestrup, J. Steffensen, H. Clausen, H. Miller, V. Masson-Delmotte, A. Sveinbjornsdottir, and J. White (2001), Oxygen isotope and palaeotemperature records from six Greenland ice-core stations: Camp Century, Dye-3, GRIP, GISP2, Renland and NorthGRIP, *J. Quat. Sci.*, *16*(4), 299–307, doi:10.1002/jqs.622.

Jones, P. D., T. Jonsson, and D. Wheeler (1997), Extension to the North Atlantic Oscillation using early instrumental pressure observations from Gibraltar and south-west Iceland, *Int. J. Climatol.*, *17*(13), 1433–1450, doi:10.1002/(SICI)1097-0088(19971115)17:13<1433::AID-JOC203>3.0.CO;2-P.

Joussaume, S., R. Sadourny, and J. Jouzel (1984), A general-circulation model of water isotope cycles in the atmosphere, *Nature*, *311*(5981), 24–29, doi:10.1038/311024a0.

Jouzel, J., G. Russel, R. Suossu, R. Koster, J. White, and W. Broecker (1987), Simulations of the HDO and $H_2^{18}O$ atmospheric cycles using the NASA GISS general-circulation model: The seasonal cycle for present-day conditions, *J. Geophys. Res.*, *92*(D12), 14,739–14,760, doi:10.1029/JD092iD12p14739.

Jouzel, J., G. Hoffmann, R. Koster, and V. Masson (2000), Water isotopes in precipitation: Data/model comparison for present-day and past climates, *Quat. Sci. Rev.*, *19*(1-5), 363–379.

Kiilsholm, S., J. Christensen, K. Dethloff, and A. Rinke (2003), Net accumulation of the Greenland ice sheet: High resolution modeling of climate changes, *Geophys. Res. Lett.*, *30*(9), 1485, doi:10.1029/2002GL015742.

Leutbecher, M., and T. N. Palmer (2008), Ensemble forecasting, *J. Comput. Phys.*, *227*(7), 3515–3539, doi:10.1016/j.jcp.2007.02.014.

Majewski, D. (1991), The Europa-Modell of the Deutscher Wetterdienst, paper presented at Seminar on Numerical Methods in Atmospheric Models, Eur. Cent. for Medium-Range Weather Forecasts, Reading, U. K.

Masson-Delmotte, V., et al. (2005), Holocene climatic changes in Greenland: Different deuterium excess signals at Greenland Ice Core Project (GRIP) and NorthGRIP, *J. Geophys. Res.*, *110*, D14102, doi:10.1029/2004JD005575.

Masson-Delmotte, V., et al. (2008), A review of Antarctic surface snow isotopic composition: Observations, atmospheric circulation, and isotopic modeling, *J. Clim.*, *21*(13), 3359–3387, doi:10.1175/2007JCLI2139.1.

Mathieu, R., D. Pollard, J. Cole, J. White, R. Webb, and S. Thompson (2002), Simulation of stable water isotope variations by the GENESIS GCM for modern conditions, *J. Geophys. Res.*, *107*(D4), 4037, doi:10.1029/2001JD900255.

Noone, D., and I. Simmonds (2002), Associations between delta O-18 of water and climate parameters in a simulation of atmospheric circulation for 1979–95, *J. Clim.*, *15*(22), 3150–3169.

North, G., T. Bell, R. Cahalan, and F. Moeng (1982), Sampling errors in the estimation of empirical orthogonal functions, *Mon. Weather Rev.*, *110*(7), 699–706.

Otto-Bliesner, B., et al. (2006), Simulating arctic climate warmth and icefield retreat in the last interglaciation, *Science*, *311*(5768), 1751–1753, doi:10.1126/science.1120808.

Risi, C., S. Bony, F. Vimeux, and J. Jouzel (2010), Water-stable isotopes in the LMDZ4 general circulation model: Model evaluation for present-day and past climates and applications to climatic interpretations of tropical isotopic records, *J. Geophys. Res.*, *115*, D12118, doi:10.1029/2009JD013255.

Schuenemann, K. C., J. J. Cassano, and J. Finnis (2009), Synoptic forcing of precipitation over Greenland: Climatology for 1961–99, *J. Hydrometeorol.*, *10*(1), 60–78, doi:10.1175/2008JHM1014.1.

Semmler, T. (2002), Der Wasser- und Energiehaushalt der arktischen Atmosphäre, Ph.D. thesis, Max-Planck-Inst. für Meteorol., Hamburg, Germany.

Shuman, C., R. Alley, S. Anandakrishnan, J. White, P. Grootes, and C. Stearns (1995), Temperature and accumulation at the Greenland Summit: Comparison of high-resolution isotope profiles and satellite passive microwave brightness temperature trends, *J. Geophys. Res.*, *100*(D5), 9165–9177, doi:10.1029/95JD00560.

Shuman, C., D. Bromwich, J. Kipfstuhl, and M. Schwager (2001), Multiyear accumulation and temperature history near the North Greenland Ice Core Project site, north central Greenland, *J. Geophys. Res.*, *106*(D24), 33,853–33,866.

Slonosky, V., and P. Yiou (2001), The North Atlantic Oscillation and its relationship with near surface temperature, *Geophys. Res. Lett.*, *28*(5), 807–810, doi:10.1029/2000GL012063.

Sodemann, H., V. Masson-Delmotte, C. Schwierz, B. M. Vinther, and H. Wernli (2008), Interannual variability of Greenland winter precipitation sources: 2. Effects of North Atlantic Oscillation variability on stable isotopes in precipitation, *J. Geophys. Res.*, *113*, D12111, doi:10.1029/2007JD009416.

Steen-Larsen, H., et al. (2011), Understanding the climatic signal in the water stable isotope records from the NEEM shallow firn/ice cores in northwest Greenland, *J. Geophys. Res.*, *116*, D06108, doi:10.1029/2010JD014311.

Sturm, C., G. Hoffmann, and B. Langmann (2007), Simulation of the stable water isotopes in precipitation over South America: Comparing regional to global circulation models, *J. Clim.*, *20*(15), 3730–3750, doi:10.1175/JCLI4194.1.

Sturm, K., G. Hoffmann, B. Langmann, and W. Stichler (2005), Simulation of delta O-18 in precipitation by the regional circulation model REMOiso, *Hydrol. Process.*, *19*(17), 3425–3444, doi:10.1002/hyp.5979.

Tjernstrom, M., et al. (2005), Modelling the arctic boundary layer: An evaluation of six arcmip regional-scale models using data from the Sheba project, *Boundary Layer Meteorol.*, *117*(2), 337–381, doi:10.1007/s10546-004-7954-z.

Uppala, S., et al. (2005), The ERA-40 re-analysis, *Q. J. R. Meteorol. Soc.*, *131*(612), 2961–3012, doi:10.1256/qj.04.176.

Vinther, B., S. Johnsen, K. Andersen, H. Clausen, and A. Hansen (2003), NAO signal recorded in the stable isotopes of Greenland ice cores, *Geophys. Res. Lett.*, *30*(7), 1387, doi:10.1029/2002GL016193.

Vinther, B. M., K. K. Andersen, P. D. Jones, K. R. Briffa, and J. Cappelen (2006), Extending Greenland temperature records into the late eighteenth century, *J. Geophys. Res.*, *111*, D11105, doi:10.1029/2005JD006810.

Vinther, B. M., et al. (2009), Holocene thinning of the Greenland ice sheet, *Nature*, *461*(7262), 385–388, doi:10.1038/nature08355.

Vinther, B., P. Jones, K. Briffa, H. Clausen, K. Andersen, D. Dahl-Jensen, and S. Johnsen (2010), Climatic signals in multiple highly resolved stable isotope records from Greenland, *Quat. Sci. Rev.*, *29*(3-4), 522–538, doi:10.1016/j.quascirev.2009.11.002.

von Storch, H., H. Langenberg, and F. Feser (2000), A spectral nudging technique for dynamical downscaling purposes, *Mon. Weather Rev.*, *128*(10), 3664–3673.

Walker, G., and E. Bliss (1932), World Weather V, *Mon. Weather Rev.*, *4*, 53–84.

Walsh, J. E., W. L. Chapman, V. Romanovsky, J. H. Christensen, and M. Stendel (2008), Global climate model performance over Alaska and Greenland, *J. Clim.*, *21*(23), 6156–6174, doi:10.1175/2008JCLI2163.1.

Wang, X. L., V. R. Swail, and F. W. Zwiers (2006), Climatology and changes of extratropical cyclone activity: Comparison of ERA-40 with NCEP-NCAR reanalysis for 1958–2001, *J. Clim.*, *19*(13), 3145–3166.

Werner, M., and M. Heimann (2002), Modeling interannual variability of water isotopes in Greenland and Antarctica, *J. Geophys. Res.*, *107*(D1), 4001, doi:10.1029/2001JD900253.

Werner, M., U. Mikolajewicz, M. Heimann, and G. Hoffmann (2000), Borehole versus isotope temperatures on Greenland: Seasonality does matter, *Geophys. Res. Lett.*, *27*(5), 723–726.

Werner, M., M. Heimann, and G. Hoffmann (2001), Isotopic composition and origin of polar precipitation in present and glacial climate simulations, *Tellus, Ser. B*, *53*(1), 53–71.

White, J., L. Barlow, D. Fisher, P. Grootes, J. Jouzel, S. Johnsen, M. Stuiver, and H. Clausen (1997), The climate signal in the stable isotopes of snow from Summit, Greenland: Results of comparisons with modern climate observations, *J. Geophys. Res.*, *102*(C12), 26,425–26,439.

Yoshimura, K., M. Kanamitsu, D. Noone, and T. Oki (2008), Historical isotope simulation using Reanalysis atmospheric data, *J. Geophys. Res.*, *113*, D19108, doi:10.1029/2008JD010074.

Yoshimura, K., M. Kanamitsu, and M. Dettinger (2010), Regional downscaling for stable water isotopes: A case study of an atmospheric river event, *J. Geophys. Res.*, *115*, D18114, doi:10.1029/2010JD014032.

G. Hoffmann, Institute for Marine and Atmospheric Research Utrecht, Utrecht University, NL-3508 TC Utrecht, Netherlands.

S. J. Johnsen, J. Sjolte, and B. M. Vinther, Centre for Ice and Climate, Niels Bohr Institute, Juliane Maries Vej 30, DK-2100 Copenhagen, Denmark. (jesjolte@nbi.ku.dk)

V. Masson-Delmotte, LSCE (CEA-CNRS-UVSQ-IPSL), CEA Saclay, Bat 701 L'Orme des Merisiers, Gif sur Yvette, F-91191, France.

C. Sturm, Bert Bolin Centre for Climate Research, Institute for Geology and Geochemistry, Stockholm University, SE-10691 Stockholm, Sweden.